STARS

University of Central Florida
STARS

Electronic Theses and Dissertations, 2004-2019

2011

Infrared Emission Spectroscopy Of Hot Carbon Monoxide

Farnood Khalilzadeh Rezaie
University of Central Florida

 Part of the Physics Commons
Find similar works at: https://stars.library.ucf.edu/etd
University of Central Florida Libraries http://library.ucf.edu

This Masters Thesis (Open Access) is brought to you for free and open access by STARS. It has been accepted for inclusion in Electronic Theses and Dissertations, 2004-2019 by an authorized administrator of STARS. For more information, please contact STARS@ucf.edu.

STARS Citation
Rezaie, Farnood Khalilzadeh, "Infrared Emission Spectroscopy Of Hot Carbon Monoxide" (2011). *Electronic Theses and Dissertations, 2004-2019*. 1858.
https://stars.library.ucf.edu/etd/1858

INFRARED EMISSION SPECTROSCOPY OF HOT CARBON MONOXIDE

by

FARNOOD KHALILZADEH REZAIE
B.S., University Of Tehran, 2009

A thesis submitted in partial fulfillment of the requirements
for the degree of Master of Science
in the Department of Physics
of College of Sciences
at the University of Central Florida
Orlando, Florida

Major Professor: Robert E. Peale

Summer Term
2011

©2011 Farnood Khalilzadeh Rezaie

ABSTRACT

Gas giant exoplanets known as hot Jupiters orbit close to their parent stars and are heated to high temperatures. Their infrared spectra, measured by photometry during secondary eclipses, are dominated by carbon monoxide and methane, the principle reservoirs of carbon on these planets. The relative CO and CH_4 abundances inform us about temperature and pressure conditions and also about mixing by global winds driven by intense but asymmetric heating for these tidally locked bodies. Emission spectra collected during secondary eclipses, as the hot Jupiter passes behind its parent star, in principle allows a determination of the CO:CH_4 concentration ratio. Since hot Jupiters exist at temperatures of order 700 K, accurate model atmospheres require high temperature line lists for relevant molecules, for which existing data bases are apparently incomplete. Since the outer atmospheres of hot Jupiters are bombarded by intense ultraviolet radiation and energetic particles, there may even be a significant degree of ionization and non-equilibrium populations among the various molecular levels. Here we present high temperature emission spectra of CO obtained from a microwave discharge plasma, where the source of CO was carbon dioxide that dissociates under microwave heating. The spectrum was measured in the range 1800-2400 cm^{-1} at a resolution of 0.1 cm^{-1}. Vibrational transitions originating in up to the 13^{th} vibrational level of the X $^1\Sigma^+$ ground electronic term were observed. From the J values for maximum intensity lines within the rotational fine structure, we obtain a temperature estimate of ~700 K, which is comparable to the atmospheric conditions of hot-Jupiters.

Dedicated to my family

ACKNOWLEDGMENTS

I wish to acknowledge my advisor, Professor Robert Peale, for his time and advice given to me which helped shape this thesis. Without his help and patience, this work would never have been finished. I also wish to thank him for his guidance during my research.

I would like to thank Dr. Daniel Britt and Dr. Yan Fernandez for being on my dissertation committee and evaluating this work. I especially wish to thank Dr. Chandana Ghosh, Dr. Andrey Muraviev and Mr. Chris Fredricksen for their invaluable help during the analysis of the experimental spectrum.

I would also wish to thank my fellow group members, Pedro Figueiredo and Jonathan Arnold for making the experimental setup. I would also like to thank my friends and group members, Mehdi Ashrafi, Maral Aminpour, Gautam Medhi, Max Moeller, Deep Panjawani, Evan Smith, Tatiana Brusentsova, Janardan Nath, Monas Shahzad and Nima Nader.

TABLE OF CONTENTS

LIST OF FIGURES

INTRODUCTION

Hot Jupiters are extra solar planets whose masses are near to or exceed that of Jupiter and which orbit close to their parent star. Among exoplanets, Hot Jupiters are the type easiest to find. Emphasis is shifting from discovering near planets to understanding their exotic atmospheres and chemistry via infrared emission spectroscopy.

Hydrogen and helium are supposed the most abundant molecules in extrasolar planets based on assumed solar abundances, but these have no infrared signature. Carbon, Nitrogen and Oxygen are relatively minor constituents, but the molecules formed from them dominate the infrared spectrum.

In “Hot Jupiters”, Carbon is thought to be sequestered primarily in Carbon Monoxide and Methane. The relative CO and CH_4 abundances inform us about temperature and pressure conditions [1] and also about mixing by global winds driven by intense but asymmetric heating for these tidally-locked bodies. Emission spectra are collected during secondary eclipses, as the hot Jupiter passes behind its parent star. These spectra in principle allow a determination of the CO: CH_4 concentration ratio.

Interpretation of exoplanet emission spectra requires comparison to model atmospheres based on laboratory molecular spectra. Modelers depend on lists of transition frequencies, line widths and

intensities that are tabulated in public data bases, such as HITRAN [2] and Spectra factory [3]. Since Hot Jupiters exist at temperatures of order 1000 K, accurate model atmospheres require high temperature line lists for those molecules, for which existing data bases are apparently incomplete.

In addition to its importance in extra solar research, hot CO emission is found in other astronomical objects such as Disks and Jets. The fundamental ro-vibtrational line spectrum of CO can be readily detected in astronomical objects from ground based observations. This makes CO an optimal tracer for characteristics of the warm gas in the inner regions of disks [4]. CO overtone emission was detected for the first time in low and high mass young stellar objects by Thompson [5] and was attributed to circumstellar disk by Carr [6].

The isotopic composition of $^{12}C^{16}O$ makes up over 99% of all CO molecules, but lines of other isotopes also can be detected when the emission is sufficiently strong [7]. Relative line strengths provide insight into excitation mechanisms for the emission [4].

CO emission spectra typically show nearly symmetric rotational sideband structure. In hot CO, excited vibrational states are occupied, such that transitions (V(21), V(32), etc) may be observed in addition to the V(10) band. Fundamental CO V(10) emission has been observed from disks of T Turi stars [7,8]. The same band also has been reported for Ae/Be stars [9, 10]. The fundamental V(10) ro-vibrational emission of CO is excited at 1000-1500 K temperature. The V(20) emission reported [4] requires significantly higher temperature [4].

The observation of CO in protoplanetary disks has been recently reported [11]. Carbon monoxide fundamental emission V(10) has been detected for all of these disks. Also, all of those disks have shown V(21) emission bands while half of these objects have been observed with up to V=4 transitions (i.e., V(43), V(32)). Excitation analysis of the integrated line fluxes reveal a significant difference between typical rotational and vibrational temperatures, suggesting that at least some of the emission is photoexcited by UV rather than being all thermal emission from a gas cloud in thermal equilibrium.

The recent analysis of the observations of Spitzer space telescope in 5-37 micron region shows the molecular spectrum of CO with emission lines in protoplanetary disks [12]. The spectrum also shows a rising continuum around 5 micron wavelength, which would be interpreted as unresolved emission lines from highly excited rotational levels of the CO V(10) fundamental band. Additionally, the pure rotational emission from CO V(21) has been detected.

To summarize, CO has a significant role in astronomical observations. The current line list of hot CO is incomplete. Accurate analysis of astronomical IR spectra will require a complete and broad line list for CO corresponding to high temperatures and non-equilibrium populations of excited states. This thesis explores our hypothesis that microwave discharge spectroscopy of CO allows experimental access to the required transitions and can contribute new information to publicly accessible line lists.

In this thesis, I present a high temperature emission spectrum of CO and partial analysis. Populations within rotational manifolds of a given vibrational level are thermalized with

temperatures approaching 700 K. On the other hand, observation of emission from vibrational levels of quantum number as high as 13 indicate that populations among these levels are far from equilibrium. The temperature corresponding to translational degrees of freedom, as determined by Doppler line widths, is found to be close to room temperature.

CHAPTER ONE: THE CO MOLECULE

1.1 Energy levels

Carbon Monoxide is a diatomic molecule and contains one atom of Carbon and one atom of Oxygen covalently bonded. The possible electronic terms in Carbon Monoxide are $2\ ^{1,3,5}\Sigma^{+}$, $^{1,3,5}\Sigma^{-}$, $2\ ^{1,3,5}\Pi$, and $^{1,3,5}\Delta$. The number 2 in front of two of the terms says that there exist two such terms. The superscript to the left of the capital Greek letters gives the spin multiplicity 2S+1. The Greek letters themselves indicate the value of Λ, the projection of the orbital angular momentum on the molecular axis. The sign superscripts to the right of the Σ terms give the sign of the wavefunction under reflection in a "vertical" plane that contains the molecular axis. The ground term of the CO molecule is represented by $X\ ^{1}\Sigma^{+}$. This is a spin singlet (S = 0) and the wavefunction does not change sign under reflection in the vertical plane [13, 14].

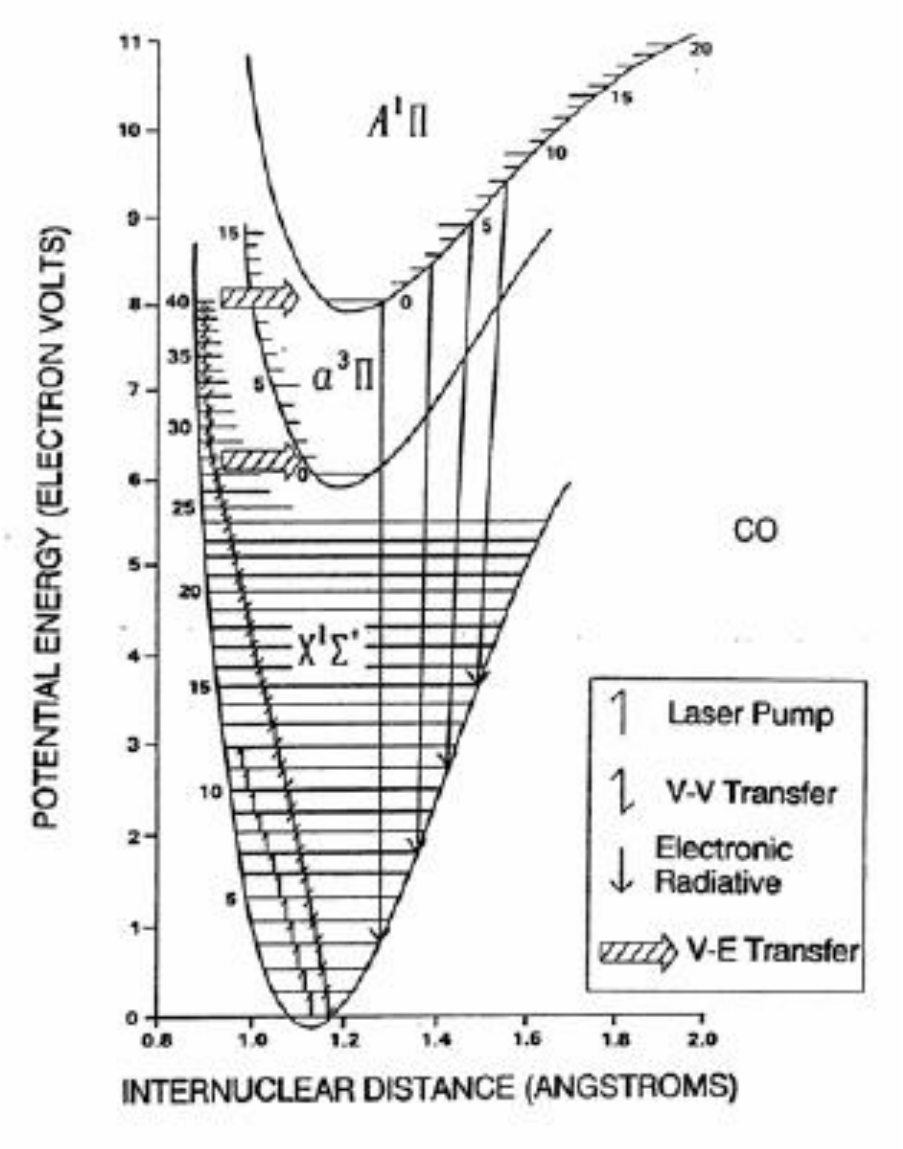

Figure 1. Potential energy of CO, showing first three electronic terms and their vibrational levels [14].

Fig 1 presents the term energies as a function of molecular bond length r for the lowest three terms. Each has a minimum at a particular value of r. Near the minimum the potential is nearly quadratic in r, giving rise to a simple harmonic oscillator spectrum. The vibrational energy

levels belonging to the ground and first two excited terms are indicated in Fig.1. The first excited term of CO is denoted $a^3\Pi$, and the next, which has the same multicipility as the ground term, is called $A^1\Pi$ [13, 14]. Since in our experiment, a plasma with significant ionization is produced, there is a chance that IR emission between vibrational levels of excited electronic terms might be observed. This hypothesis has not yet been confirmed by our partial analysis of the spectrum. So far, the strongest emission features are largely interpreted as belonging to the X $^1\Sigma^+$ term.

1.2 Vibrational energy levels

The models of rigid rotor and anharmonic oscillator explain the main characteristics of the infrared spectra of CO. The anharmonic Morse potential is characteristically parabolic near its minimum but the restoring force increases rapidly at distances shorter than the equilibrium separation and approaches zero as the atomic separation becomes larger. These features are shown in Fig. 2 which compares the Morse potential to the harmonic potential. In the Morse potential, the vibrational levels G(V) = E(V)/hc are not evenly spaced, as they are in the harmonic potential. Instead, the separation between neighboring levels decreases as the vibrational quantum number and energy increase.

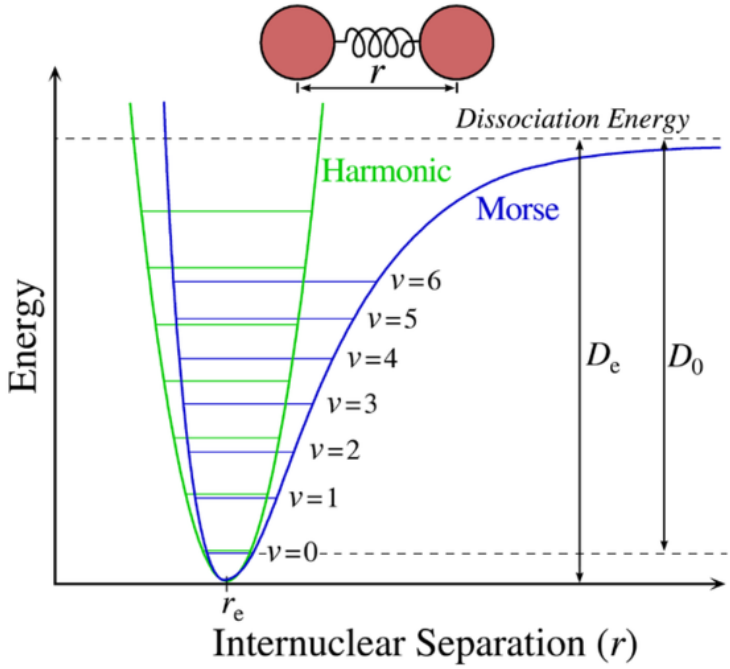

Figure 2. Energy diagram of CO molecule.

In the neighborhood of the minimum, the Morse potential approximates a parabola (Green curve in Fig. 2). Nevertheless, the effect of the anharmonicity is very large compared to both the spectral width of the observed emission lines and the resolution of our measurements, so that (for instance) the V(10) emission band is easily distinguished from the V(21) band.

Note that the mean atomic separation in the Morse potential increases with increasing vibrational quantum number v. This means that the moment of inertia *I* is also increasing. The rotational constant $B = \frac{h}{8\pi^2 c\, I_B}$ is therefore decreasing, so that the rotational levels associated with each vibrational level get closer together for higher vibrations. This effect is also clearly observed in our experiment. This is represented by replacing B with B_v which is the rotational constant for vibrational state V and is slightly smaller than B_e which corresponds to equilibrium separation r_e . This is expressed quantitatively as

$$B_v = B_e - \alpha_e (V+1/2) , \qquad (1.1)$$

where α_e is a constant smaller than B_e .

Similarly, rotational motion tends to stretch the bond, increasing the moment of inertia. This effect is accounted for by a second rotational constant D_v, which is also a function of the vibrational quantum number according to

$$D_v = D_e + \beta_e (V+1/2) \qquad , \qquad (1.2)$$

where β_e is small compared to D_e .

The rotational energy depends on the two rotational constants and the rotational quantum number J according to

$$F_v(J) = B_v J (J+1) - D_v J^2 (J+1)^2 \quad . \qquad (1.3)$$

The centrifugal effect is seen to decrease the rotational energy as J increases.

Changes in vibrational quantum number by any integral amount are allowed due to anharmonicity, but transitions with $\Delta V = -1$ (Figure 3) give by far the most intense emission transitions. Our emission spectra are collected in a frequency region corresponding to these strong transitions.

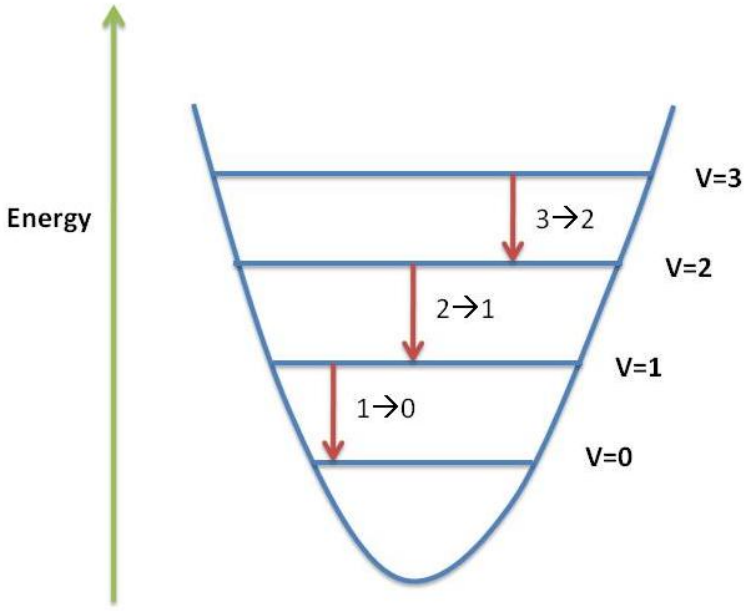

Figure 3. First three emissions with ΔV = -1 in a diatomic molecule.

Now, if we consider a particular vibrational transition from **V**' to V'' one can write for the wavenumbers of the resulting lines (neglecting for now the terms depending on D_v)

$$\nu = \nu_0 + B_v' J' (J'+1) - B_v'' J'' (J''+1), \tag{1.4}$$

where $\nu_0 = G(V')-G(V'')$ and $G(V)=E(V)/hc$. The quantity ν_0 is the frequency of the pure vibrational transition without taking account of rotation ($J'=J''=0$). Here, the quantum numbers with a single prime refer to the upper (initial) level for the emission, and those with double prime denote the lower (final) level, so that ν_0 is a positive number. With selection rules $\Delta J = +1$ and $\Delta J = -1$ respectively, we obtain

$$\nu_R = \nu_0 + 2 B_{v'} + (3 B_{v'} - B_{v''}) J + (B_v' - B_v'') J^2 \text{ , with } J = 0, 1, 2,\ldots \tag{1.5}$$

$$\nu_P = \nu_0 - (B_{v'} + B_{v''}) J + (B_{v'} - B_{v''}) J^2 \text{ , with } J = 1, 2, 3,\ldots \tag{1.6}$$

Here J = J'' is the rotational quantum number of the lower level. These two formulas represent the lines of the ro-vibrational bands referred to as the R and P branches, respectively. The P branch always occurs at lower wavenumbers than the R branch.

The smallest value of J in the R branch is 0 while in the P branch it is 1. This spectrum is represented schematically by Fig. 4.

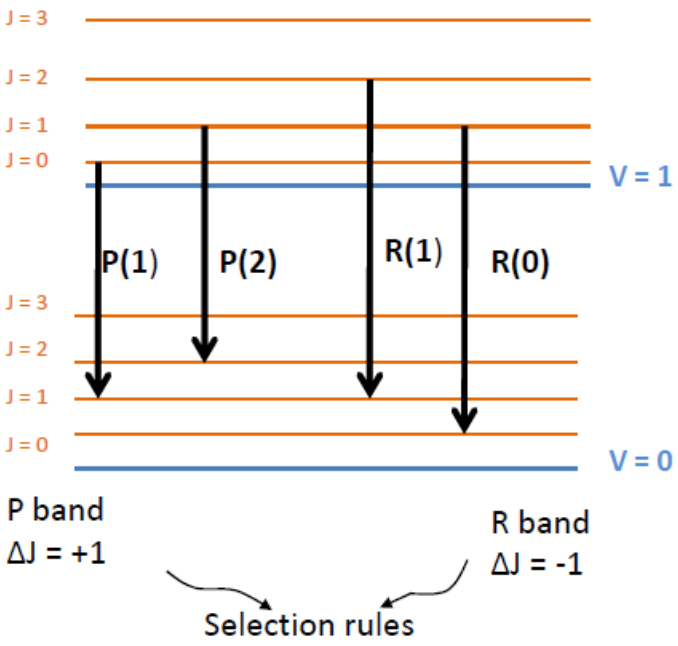

Figure 4. Energy level diagram explaining a rotation-vibration band of V(10) transition.

The two branches of R and P can be combined into a single formula

$$\nu_{PR} = \nu_0 - B_{v'} + (B_{v'} + B_{v''})m + (B_{v'} - B_{v''})m^2 \quad , \qquad (1.7)$$

Where m is an integer which takes values 1, 2, 3,… for the R band (that is m = J+1) and the values -1,-2,-3,… for the P band (that is m = -J). Then, selection rules prevent the occurrence of a transition having m = 0. This missing line is located at the frequency ν_0, and is called the "Zero line" or "Band Origin".

Inclusion of the D terms introduces a correction to the term second order in m and also new terms involving third and forth powers of m. We find it absolutely necessary to include terms up to the third power of m in order to explain the experimental spectrum. Terms of 4^{th} power of m give corrections much smaller than our experimental resolution and can be ignored.

1.3 Thermal distribution of population in energy levels

The emission intensities of individual ro-vibrational lines depend mainly on the number of molecules in the initial levels, which are determined by Boltzmann statistics for thermally populating the levels available to the ensemble of CO molecules. This assumes that thermal equilibrium holds. Actually, in our apparatus, in which microwaves continually pump the gas, causing ionization and collisional excitations, the various degrees of freedom appear to be not in thermal equilibrium with each other. However there seems to exist thermal equilibrium within the rotational levels, at least. In other words, the populations of rotational levels belonging to the initial (upper) vibrational level are determined by a Boltzmann factor with a given temperature, though the value of this temperature may be differ significantly from the one corresponding to translational motion, as determined from Doppler line widths.

According to "Maxwell-Boltzmann distribution law", the number of molecules d_{N_E} that have energy between E and E + dE is exp(-E/kT) dE, where k is Boltzmann's constant and T is the absolute temperature.

The number of molecules in vibrational level V is

$$N_v = \frac{N}{Q_v} e^{-G(v)hc/kT} \quad , \tag{1.8}$$

where Q_v is the partition function and N the total number of molecules.

Even at temperatures as high as 1000 K, $Q_v \sim 1$, so that $N_v \sim N \exp[-G(V)\, hc/kT]$. However, in our discharge spectroscopy, we see emission originating from vibrational levels as high as 13, which corresponds to a temperature of ~40000 K, if thermal equilibrium were to hold. Thus, the populations of the vibrational levels in a microwave-pumped plasma discharge are very probably not in equilibrium. Rather, the emission we see from highly excited levels results from a cascade of radiative decay for CO molecules that are excited by external microwave pumping.

1.4 Rotation inside each vibrational level

The thermal distribution of rotational levels belonging to each vibrational level requires, in addition to the Boltzmann factor exp(-E(J)/kT), a degeneracy factor 2J+1. The number of molecules N_J in the rotational level J of the lowest vibrational state at the temperature T is therefore [15]

$$N_J = \text{Coeff}\ (2J+1)\ \exp[-F(J)\ hc/kT] \tag{1.9}$$

For the CO ground term ($\Lambda = 0$), assuming a rigid rotor, we have

$$N_J \propto (2J+1)e^{-BJ(J+1)hc/kT} \quad . \tag{1.10}$$

The 2J+1 factor increases with J, while the exponential factor decreases, so that the population function has a maximum at finite J. Setting $dN_J/dJ = 0$ at the maximum and solving for J_{max}, we find

$$J_{max} = \sqrt{\frac{KT}{2Bhc}} - \frac{1}{2} = 0.5896\sqrt{\frac{T}{B}} - \frac{1}{2} \tag{1.11}$$

The actual number of molecules in the rotational states is obtained by multiplying by N and dividing by the rotational partition function Q_r. For sufficiently large T this is

$$Q_r \cong \int_0^\infty (2J+1)\exp\left(-\frac{hcBJ(J+1)}{kT}\right)\ dJ = kT/hcB \tag{1.12}$$

Consequently the number of populated sates in rotational level J will be

$$N_J = N\,(hcB/kT)\,(2J+1)\,\exp[-B\,J(J+1)\,hc/kT] \qquad (1.13)$$

The variation of the intensity for the lines of rotational fine structure in a given vibrational translation depends on the thermal distribution of molecules among the rotational levels of the initial (upper) vibrational level. The J in the formula is that belonging to the initial level, namely J' for emission and J" for absorption.

Besides the population factor, transition intensities also depend on transition dipole matrix elements and on the frequency ν. The final intensity formulas for emission is

$$I_{em} = (\nu^4\, C_{em}/Q_r)\,(J'+J''+1)\,\exp[(-B'\,J'(J'+1)\,(hc/kT)] \qquad . \qquad (1.14)$$

We can replace the 2J+1 with J'+J"+1 meaning the intensity depends only on the mean value of 2J+1 [15]. Here C_{em} is a constant, which is depending on the change of dipole moment. We take this to be the same for all lines in a given band. For a given vibrational transition, the variation in frequency ν is small compared to the mean frequency, so that we may take it as constant. Then, at given temperature, the factor ($\nu^4\, C_{em}/Q_r$) is nearly constant. Therefore, the intensity distribution is mainly determined by the population factor Eq. (1.13).

In Fig 5, the theoretical intensity distribution is presented for the V(10) R and P branches of CO at 300 K and 1100 K. With increasing temperature, the band extends to higher frequency and the intensity maxima of the two branches move outward and at the same time become more flat. The decrease of the height of the maximum with increasing temperature is due to the increase of the state sum Q_r in the denominator of the expression above.

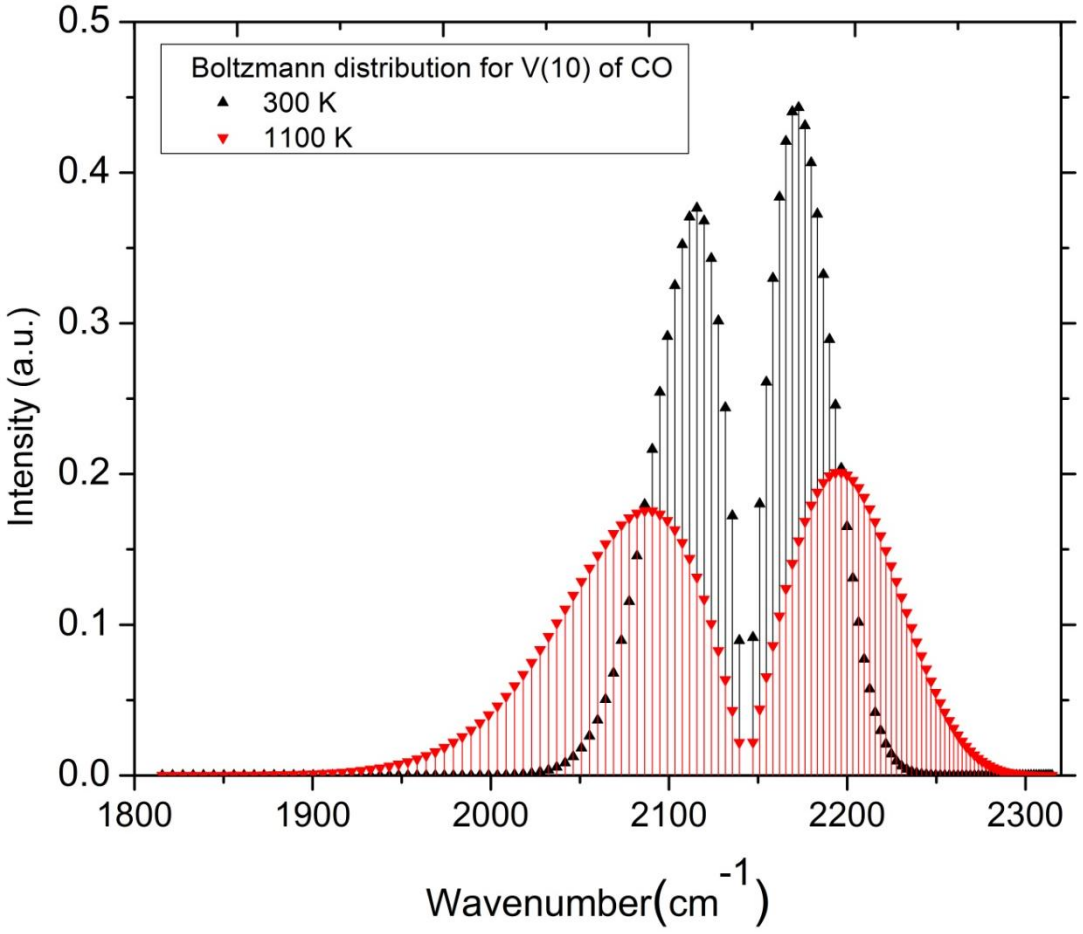

Figure 5. Amplitudes of individual P and R branch lines for the V(10) of CO at T= 300 K and T = 1100 K.

The maximum of the P and R branches can be recognized and their separation measured. A rough value for the rotational constant B may be obtained if the temperature is known. Consequently, the separation of P and R bands will be

$$\Delta v_{PR}^{max} = \sqrt{\frac{8kBT}{hc}} = 0.3583\sqrt{BT} \qquad (1.15)$$

Using the above formula gives us the same estimation for the rotational temperature of Carbon Monoxide molecules in discharged tube, since the B value is known.

The above calculations and approximations enable us to estimate the rotational temperature from the envelop of the P and R emission bands for a given vibrational transition. This assumes that the rotational populations are thermalized, which is verified by the observation that the envelops closely follow the theoretical predictions. This is in contrast to the vibrational levels, which are found to be not in thermal equilibrium. The rotational temperature determined is much higher than the translational temperatures deduced from the Doppler line widths.

1.5 Linewidth and broadening

The major line broadening mechanism is Doppler broadening. The intensity will be related to thermal temperature of molecules according to

$$I(\nu) = I_0 \exp[-(c(\nu - \nu_0)/ \nu_0 v_p)^2] \quad (1.16)$$

in which the thermal velocity of the molecule is

$$v_p = \sqrt{\frac{2kT}{M}} \quad , \quad (1.17)$$

while T is the translational temperature of the molecules, k is the Boltzmann constant, and M is the total mass of the molecule[16].

1.6 Absorption and Beer's law

The Beer-Lambert Law, more commonly known as Beer's Law, states that the optical absorbance of a molecule varies linearly with concentration. Beer's Law is the simple solution to the more general description of Maxwell's far-field equations describing the interaction of light with matter. Absorbance is measured in a spectrophotometer by passing a collimated beam of light at wavelength λ through a plane parallel slab of material that is normal to the beam. Absorbance (A_λ) is calculated from the ratio of light energy passing through the sample (I_0) to the energy that is incident on the sample (I)

$$A = -\ln(I/I_0) \tag{1.18}$$

Transmittance is given by

$$T = I/I_0 = \exp(-\sigma\, l\, N) \tag{1.19}$$

where I and I_0 are the intensity of incident and the transmitted electromagnetic wave, respectively, σ is cross section, l is the path length, and N is the number density of molecules.

CHAPTER TWO: THE EXPERIMENT

Microwave discharge creates a plasma with energetic electrons and reactive molecular fragments. This is our approach to simulating the hot and non-equilibrium conditions caused by photo-ionization of a Hot Jupiter atmosphere.

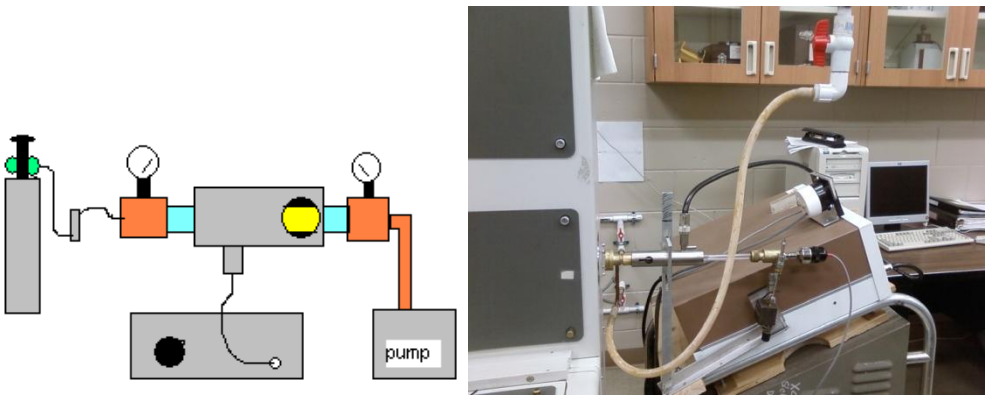

Figure 6. (left) Schematic of microwave discharge apparatus. A mixture of gases from a set of regulated gas bottles is controlled by flow meters. The pressure is measured with a gauge at the input of a quartz tube, which passes through the microwave cavity energized by a power supply. An aperture in the cavity allows for emission measurements. A second gauge measures the pressure at the output that leads to a vacuum pump. (right) Photograph of microwave discharge apparatus next to the Bomem DA8 Fourier spectrometer.

A schematic and photograph of our microwave discharge apparatus are presented in Fig. 6. Gases are passed through a length of quartz tubing, which is inserted into a cylindrical microwave cavity (Opthos). One end of the tube is connected to a vacuum pump, and pressure gauges at both ends determine the pressure and its gradient. Flow meters regulate the flow of

gases (CO_2 and CO) through the tube. An Opthos 100 W microwave generator at 2.45 GHz sustains the discharge initiated by a Tesla coil.

To initiate a discharge, the circuit is evacuated and buffer gas introduced and regulated with a valve between the vacuum pump and the gauge. The microwave generator forward power is adjusted to sustain a discharge initiated with a Tesla coil. The sample of interest is introduced slowly via a separate flow system, and the flow of sample and buffer is adjusted to maintain the discharge under the desired conditions. In the case of solid samples, once the sample is heated and begins to vaporize, pressure and gas flow are adjusted to stabilize the discharge.

The spectra were obtained using a microwave discharge apparatus where the source of CO was carbon dioxide that dissociates under microwave heating. The pressure inside the discharge tube was of order 1 Torr and the microwave power applied to the cavity was ~70 W. Emission exited the discharge tube via a ZnSe window and entered through a NaCl window the emission port of the evacuated Fourier spectrometer.

The technique that has been used to collect the data in the experiment is Fourier Transform Infrared Spectroscopy (FTIR). The infrared emission from the discharge is modulated by a Michelson interferometer, and the intensity recorded as a function of pathlength difference between the two interferometer arms. When these data are Fourier transformed, the intensity vs. wavenumber is obtained. The Fourier spectrometer used for collecting data in our experiment is a BOMEM DA8 with a maximum unapodized resolution of 0.017 cm^{-1}. The resolution chosen

for the spectrum analyzed here was 0.1 cm^{-1}, which was sufficient to resolve the Doppler widths of the individual lines. Resources used included a KBr beamsplitter and a 77 K InSb detector.

CHAPTER THREE: THE RESULTS

The spectrum of the emission from the microwave discharge tube is shown in Figure 7 for the spectral range 1800-2400 cm^{-1}. The most important emissions bands are due to CO and CO_2. The InSb detector cuts off the data around 1840 cm^{-1}. Symbols below the baseline indicate the positions of R0 from [17], and the numbers indicate the initial vibrational quantum number V'. We observe transitions from V' as high as 13 [Appendix B].

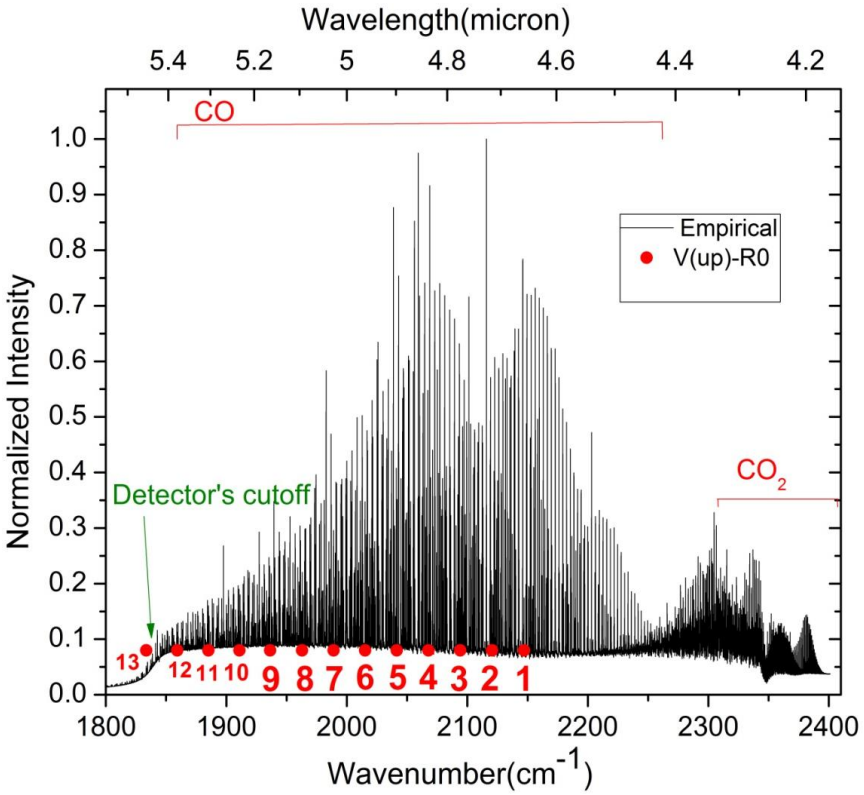

Figure 7. Microwave discharge spectrum of CO and CO_2. with the positions of R0 for vibrational states of CO up to V = 13 (with $\Delta V = -1$) are indicated by solid circular symbols.

We focus on the transitions of CO, and ignore the CO_2 spectrum from now on. We have generated the baseline using polynomial fit to its values from 1800 to 2400 cm^{-1}. The synthetic baseline is subtracted from empirical spectrum, so that all peak heights can be referenced to zero intensity.

The fundamental vibration of CO molecule V(10) is centered at 2147.08 cm^{-1}. The vibration of V (21) for CO molecule is centered at 2120.50 cm^{-1}. The individual lines within the P and R bands of these vibrations are indicated by symbols in Figure 8, where the symbols are placed at the peak maxima. These specified peaks were obtained by comparing the empirical peaks centers to HITRAN V(01) absorption transitions.

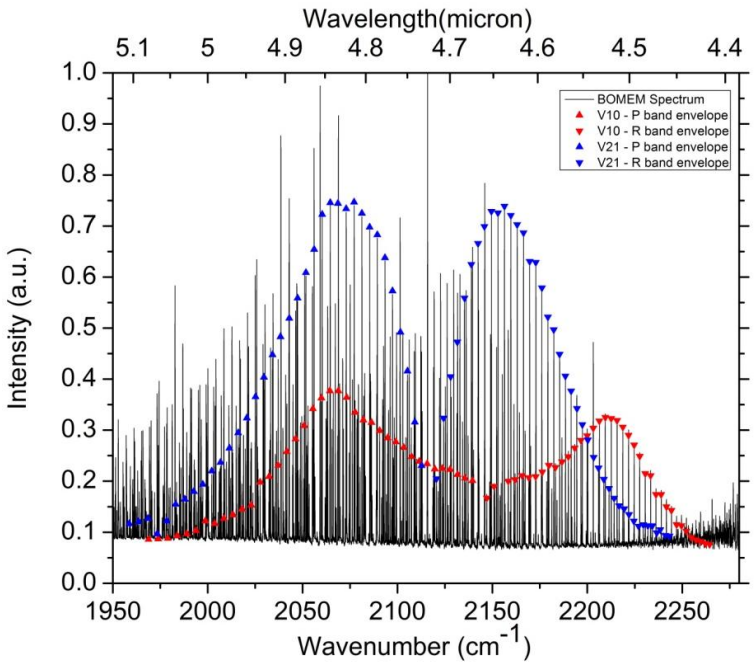

Figure 8. V(10) and V(21) emission bands of CO have been identified in the spectrum.

3.1 Fundamental vibration of CO

The observed peak centers frequencies are collected in Table 1 of the Appendix A. The peak centers are matching HITRAN database to better than our experiential resolution. However, it seems to be a systematic difference of 0.026 cm^{-1} between our values and the HITRAN values. This is an artifact due to the aging HeNe reference laser in the spectrometer, which has stabilized to the wrong longitudinal cavity mode. [2,19]. This artifact has no bearing on the subsequent analysis and it will be addressed in the future by replacing the laser.

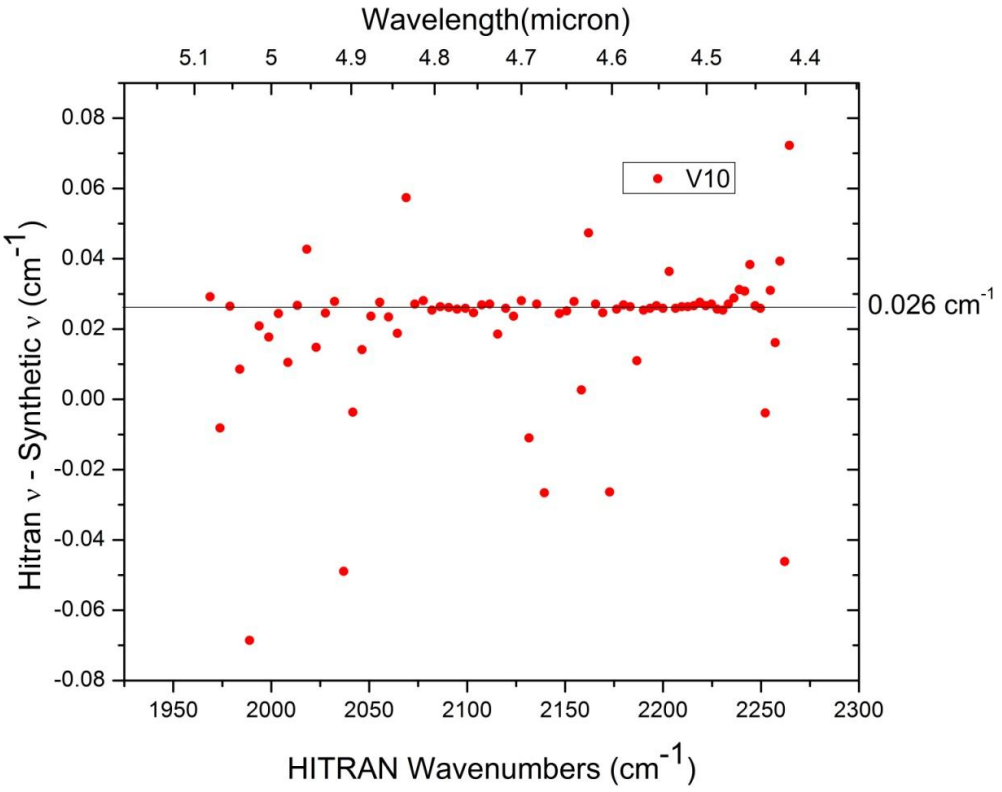

Figure 9. Difference between observed peak centers and HITRAN peaks of V(10) transition as a function of m.

In Table 1 of Appendix A, the most intense line in the R band occurs for J = 18. We are still able to observe lines in the series up to J = 38. The P band of V(10) also has a maximum intensity for J = 18. These J_{max} values are used to estimate the rotational temperature of CO molecules in a discharge tube according to Eq (1.11). We take B_{co} = 1.93 cm^{-1} and J_{max} = 18 to find the rotational temperature to be T_{rot} = 1900 K. However, we explain below why this value is artificially high due to an experimental artifact.

Table 1 of the Appendix A, also presents the P band transition values, which cover the initial states J = 0 to J = 38. The maximum intensity occurs around J = 18 and gives the same value for rotational temperature T_{rot} = 1900 K. Matching the peaks of the Boltzmann distribution of Eq (1.14) to the empirical peaks (by eye) also gives T_{rot} = 1900 K. This comparison is presented in Fig. 10.

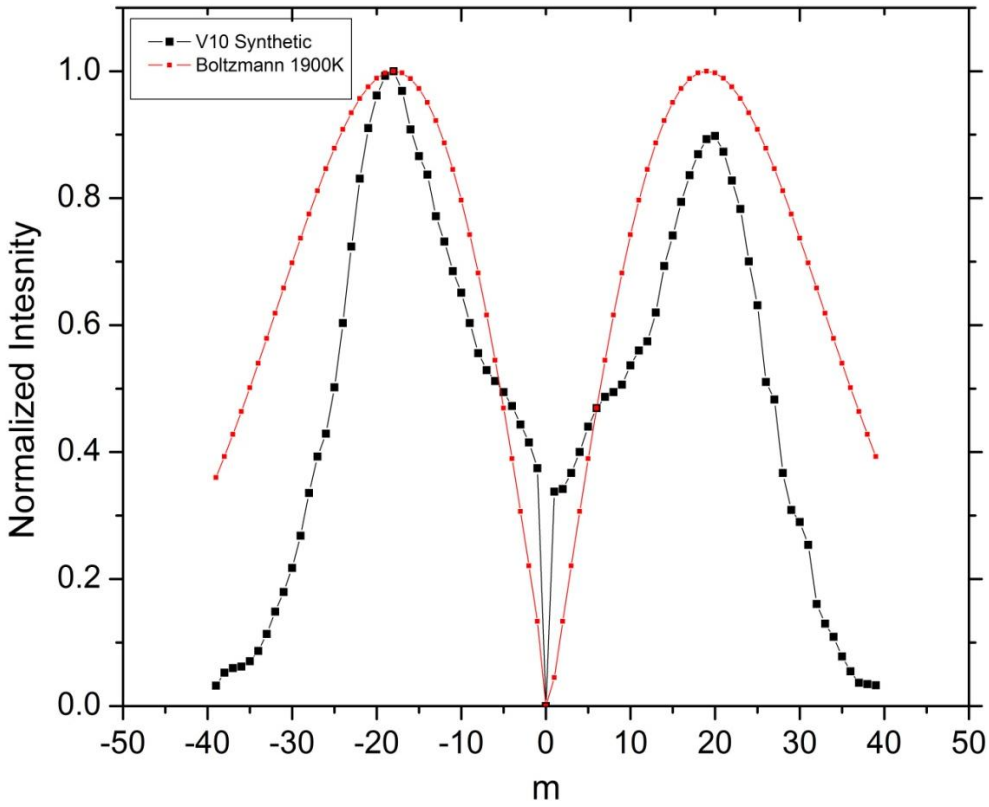

Figure 10. V(10) peak heights are shown for empirical data and for thermal equilibrium for T = 1900 K.

The agreement of the empirical envelope and the Boltzmann curves in Fig. 10 is poor. The pattern of observed peak heights for the lines belonging to V(10) do not seem to be well explained by Boltzmann distribution of the initial rotor levels.

From Fig 10, and estimation of the rotational temperature, using Eq (1.11), one can tell that empirical data points are not following the Boltzmann distribution. The explanation is that the V(10) emission is being reabsorbed by the V(10) transition of cooler CO that exits in the tube between the discharge and the exit window. Using Eqs (1.14) and and (1.19), with estimations

of 700 K and 400 K for rotational temperatures of hot and cold CO, allows us to generate a V(10) emission spectrum that is partially reabsorbed by cooler CO. We then obtain a reasonable match between empirical and simulated peak centers for V(10) transition, as shown in Fig. 11. In Figure 11, intensities of R and P branches of empirical data have been plotted together with the synthetic emission spectrum of hot CO at T = 700 K that has been partly reabsorbed by cold CO at T = 400 K. Thus, there is no need to suppose that populations of the rotational levels are not thermalized.

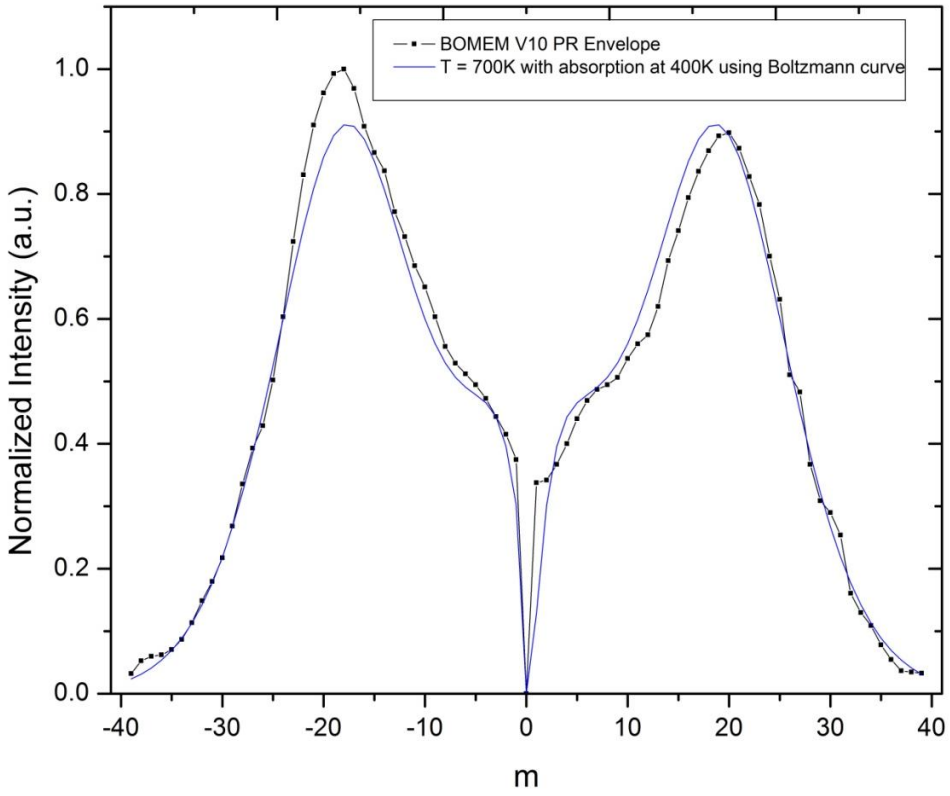

Figure 11. Empirical and synthetic band of V(10).

3.2 Linewidth and translational temperature

Here the major broadening mechanism is "Doppler broadening", which was previously introduced by Eq (1.16). Doppler broadening has a Gaussian profile and its linewidth is related to thermal velocity of molecules by Eq. (1.17).

From the width and line shape of V(10) transition, it is possible to estimate the translational temperature. Using Eq (1.16) and Eq (1.17) and matching the linewidth with empirical data, we can estimate the translational temperature of CO molecules to be T_{rot} = 290 K. Thus, rotational and translational degrees of freedom are not in thermal equilibrium.

3.3 The synthetic spectrum of V(10) transition

Up to now, we have determined the rotational and translational temperature of CO molecules with some approximations in a discharged tube. To identify transition between higher vibrational levels, we need to simplify the spectrum by subtracting those transitions that have already been identified. To do so, we generate a synthetic spectrum for the known transitions.

The synthetic spectrum for V(10) transition has been generated using a short program in FORTRAN90. The Gaussian profile has been used for generating the lineshapes. From Fig 10, we know that Boltzmann distribution and assumption of thermal equilibrium will not generate for the observed intensity distribution. So, for generating the synthetic spectrum we use the empirical intensity of each rotational line. The synthetically generated spectrum is presented in Fig 12.

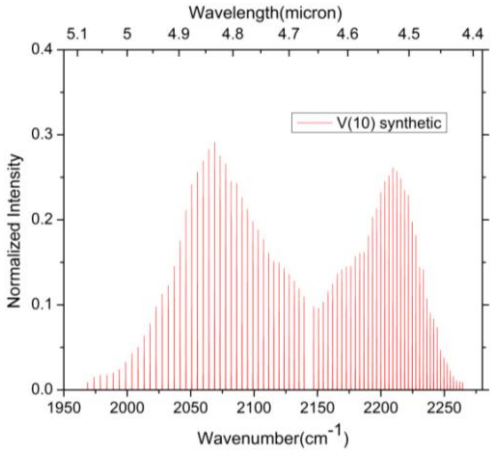

Figure 12. Synthetic spectrum of V(10) P and R branches.

In the figure above, all the intensities are matched with the empirical intensities. Details of the synthetic and empirical spectra are compared in Fig 13.

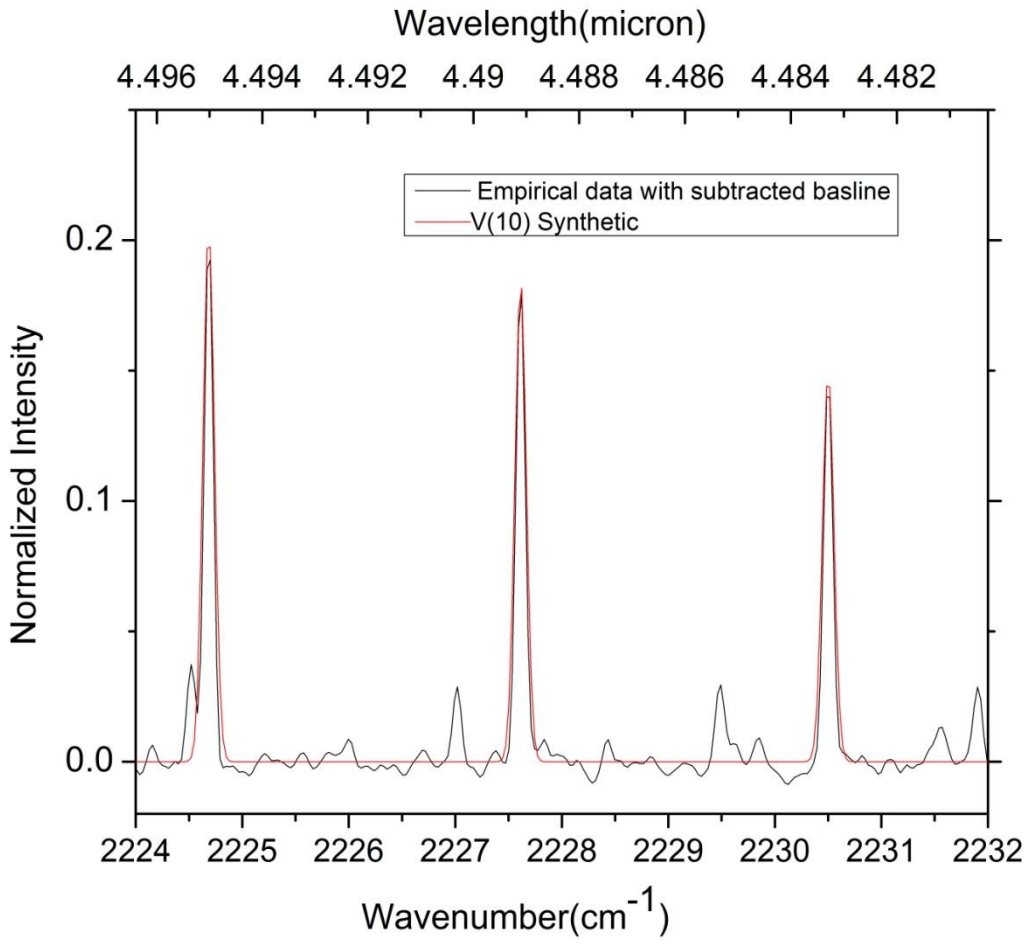

Figure 13. Synthetic V(10) R25, R26 and R27 lines are compared with the empirical spectrum, which contains additional transitions.

Fig 13 shows the synthetic V(10) R25, R26 and R27 lines in the spectrum. These bands have been plotted together with empirical spectrum which contains some additional weak lines

belonging to other vibrational transitions. It turns out that for the bands shown in the above figure, the lineshape of the synthetic spectrum is in good agreement with the empirical data.

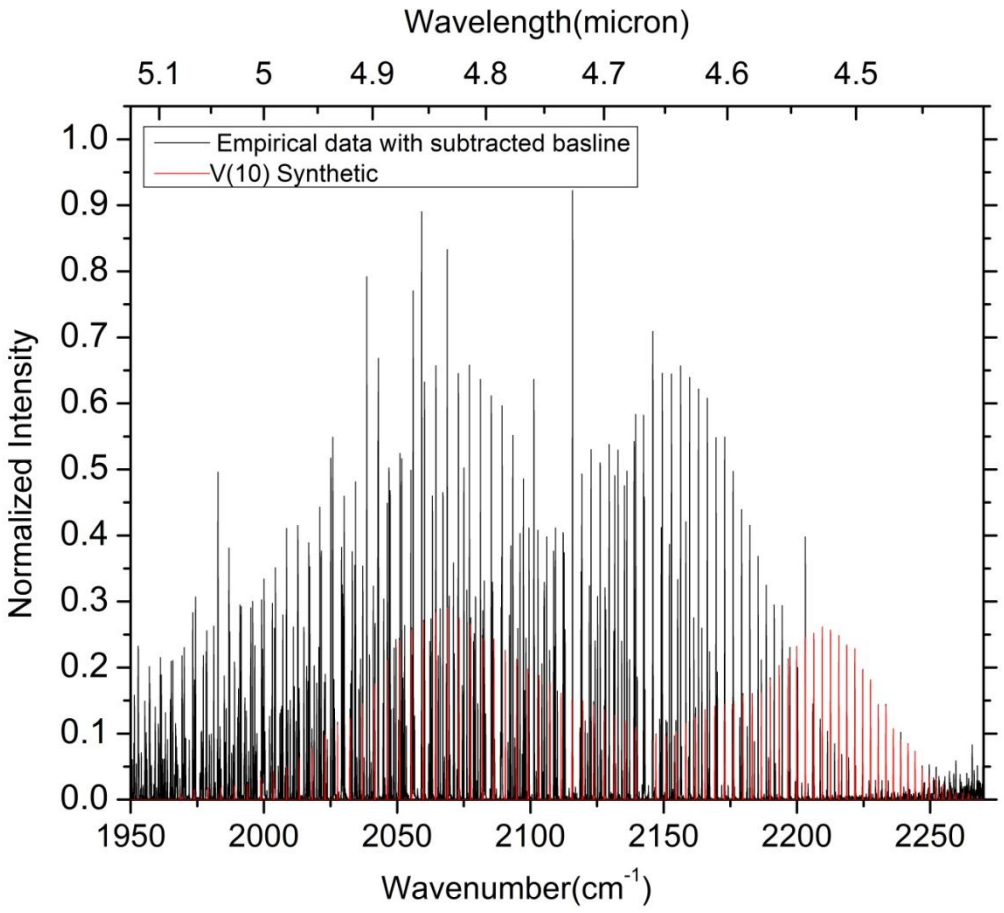

Figure 14. Synthetic V(10) spectrum and empirical data. The baseline is already subtracted.

Accidental coincidence of lines from different vibrational transitions causes some individual J lines to appear stronger than the smooth trend of their envelope. For such lines, we interpolated

between neighboring transitions that follow the monotonic trend. Such linear interpolation has been done for the R16 in the V(10) transition and the result has been shown in the Fig 15.

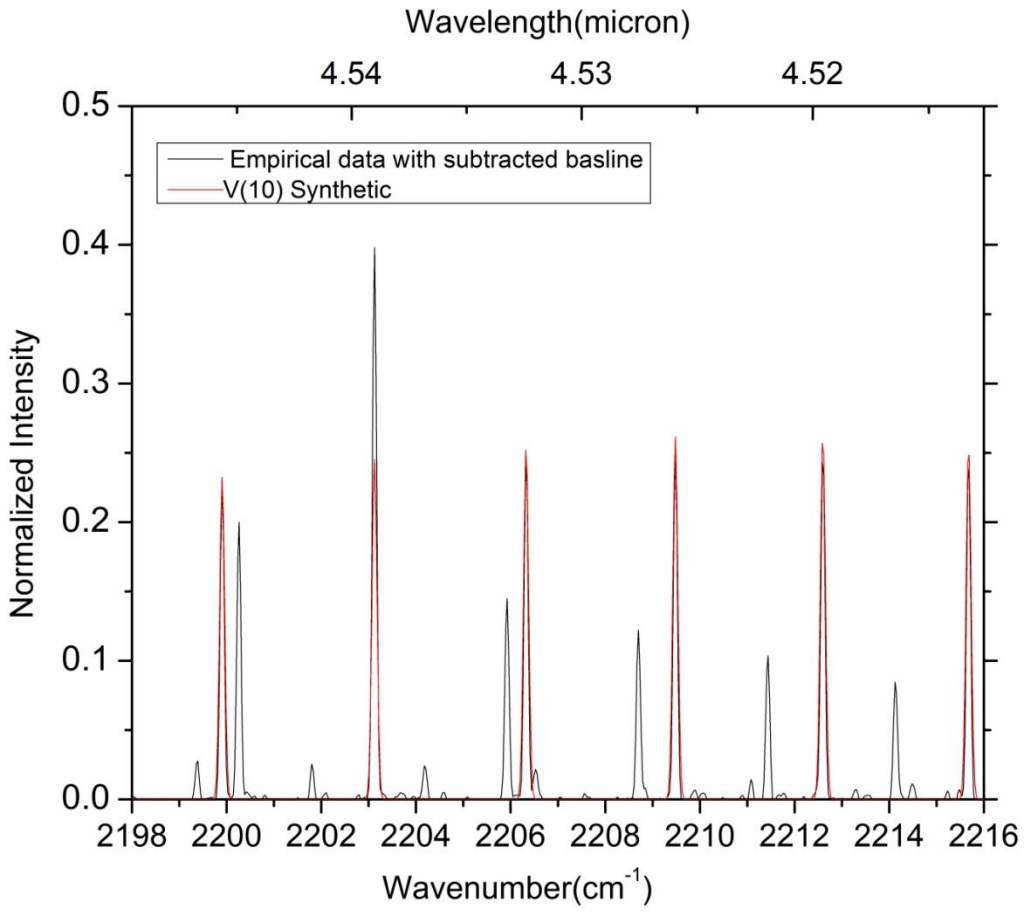

Figure 15**. Synthetic V(10) R15-R20 spectrum compared with empirical spectrum.**

The same method been used to adjust the intensity of rotational transitions and the translational temperature of T_{rot} = 290 K has been used for generating the synthetic spectrum of the P branch.

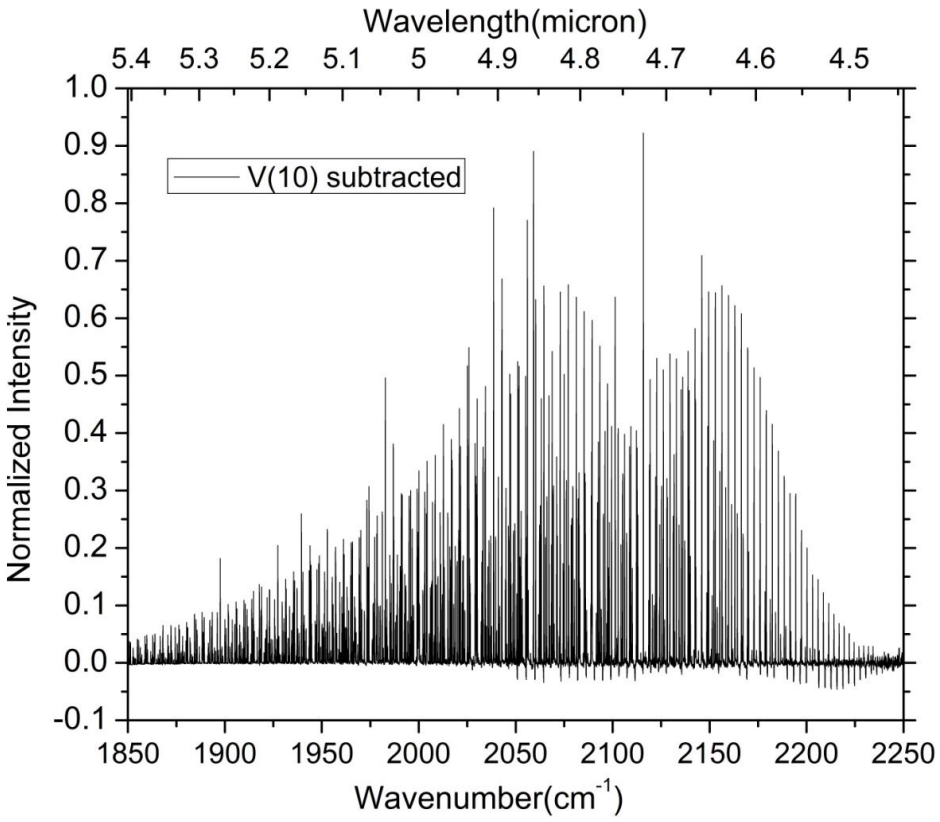

Figure 16. Empirical spectrum from which the synthetic V(10) spectrum has been subtracted.

Now, having the more realistic synthetic spectrum enables us to subtract the V(10) rotational bands from the original spectrum. The result it presented in Fig. 16. This spectrum is clearly more useful than the original spectrum for identifying the next group of lines in the spectrum.

3.4 V(21) Transition

The second vibrational band of CO molecule V(21) is centered at 2120.53 cm^{-1} and has both P and R bands. Line centers are indicated by blue symbols. Like the V(10) transition, the translational temperature of CO molecules inside the discharge tube determines the line width .

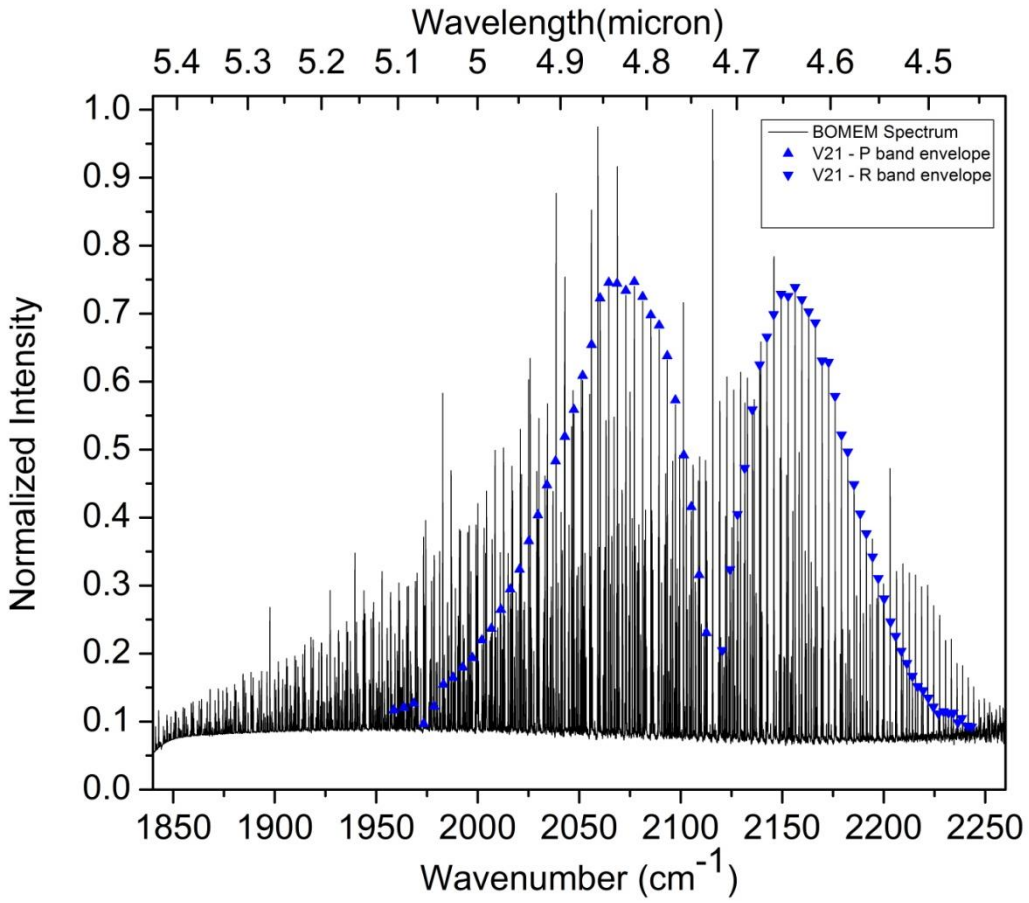

Figure 17. V(21) lines in the spectrum of the CO molecule.

In the tables 3 and 4 of Appendix A, the observed rotational bands of CO V(21) are listed with their absolute intensity and their corresponding rotational quantum number. It is clear that for J > 38 the intensity of rotational band of CO becomes very small compared to other transitions until it is no longer observable. Also from table 3 and table 4 of Appendix A, it is shown that the intensity of some rotational lines are unexpectedly high. This happens because of accidental coincidences between lines belonging to different vibrations transitions.

The first peak of V(21) transition in CO is called R0 and occurs at 2120.53 cm^{-1} with a low intensity. Gradually, the R band lines becoming more intense and finally around J = 12 we observe the highest intensity for a rotational state in the R band (around 2166.36cm^{-1}). For J > 12, the rotations become less intense, and finally around 2247.7 cm^{-1} they are not observable anymore. The P band of V(21) is similar to the R band and is extended from 1958.7 to 2112.9 cm^{-1} with a maximum intensity around J = 12, which is in agreement with the results for the R branch.

3.5 CO V(21) Transition and its lineshape

Previously we analyzed the spectrum for the V(21) transition and its relative intensity for each rotational state in P and R bands. Figure 18 shows the rotational bands for P21 and P20 centered at 2029.62 and 2034.11 cm^{-1} with the blue lines showing HITRAN peak centers. The lineshape of V(21) rotational bands are clear in the Fig 18. Similar to V(10) band, the same systematic difference in frequency (close to 0.026 cm^{-1}) is being observed between the HITRAN peaks and the observed peaks. The origin of the discrepancy is a problem with the HeNe reference laser in the spectrometer, as already mentioned.

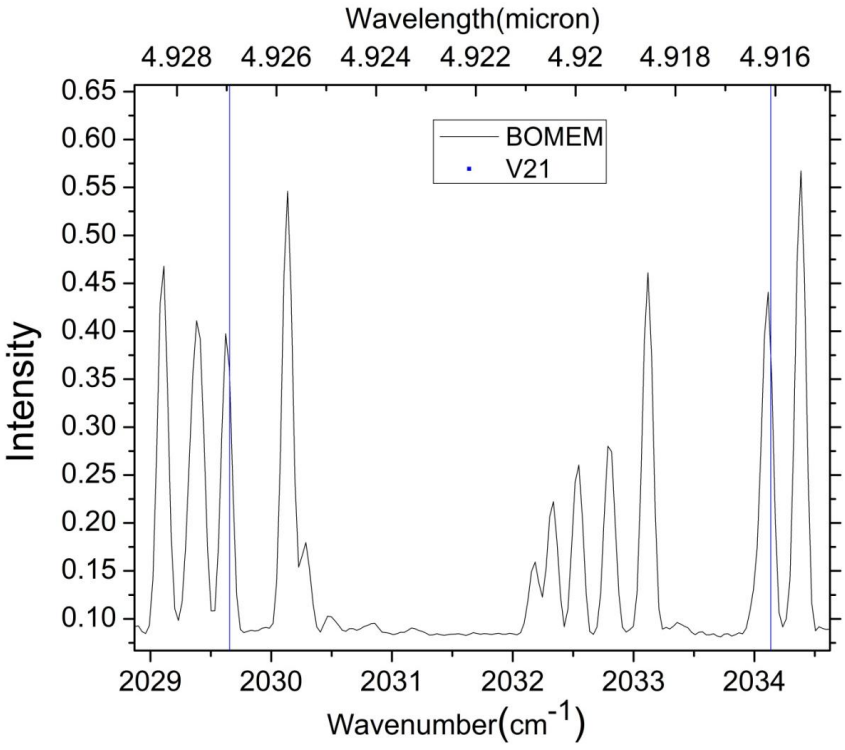

Figure 18. P21and P20 bands of V(21) with the HITRAN peak centers indicated.

Eq (1.17) determines the rotational temperature of V(10) to be T_{rot} = 700 K. Matching the peaks of the Boltzmann distribution of Eq (1.14) to the empirical peaks (by eye) gives T_{rot} = 700 K. The agreement of the empirical envelope and the Boltzmann curves is good, as shown in Fig. 19. The pattern of observed peak heights for the lines belonging to V(21) seems to be well explained by Boltzmann distribution of the initial rotor levels. For the V(21) transition, unlike V(10) , no reabsorption by V(12) transitions can occur, because the initial V=1 level for that absorption is not thermally populated at 400 K.

3.6 Linewidth and translational temperature of V(21) transition

In the V(21) band, like for V(10), each peak in the spectrum has a lineshape and a specific width. Based on the same calculations done for V(10) and using the width of V(21) rotational bands, we can estimate the translational temperature of those molecules which are contributing to V(21) transition: T_{tran} = 290 K. The results are in agreement with translational temperature found from the V(10) lines. From now, our focus will be to generate the best possible synthetic spectrum of V(21) transition using the T_{rot}= 700 K and T_{tran} = 290 K.

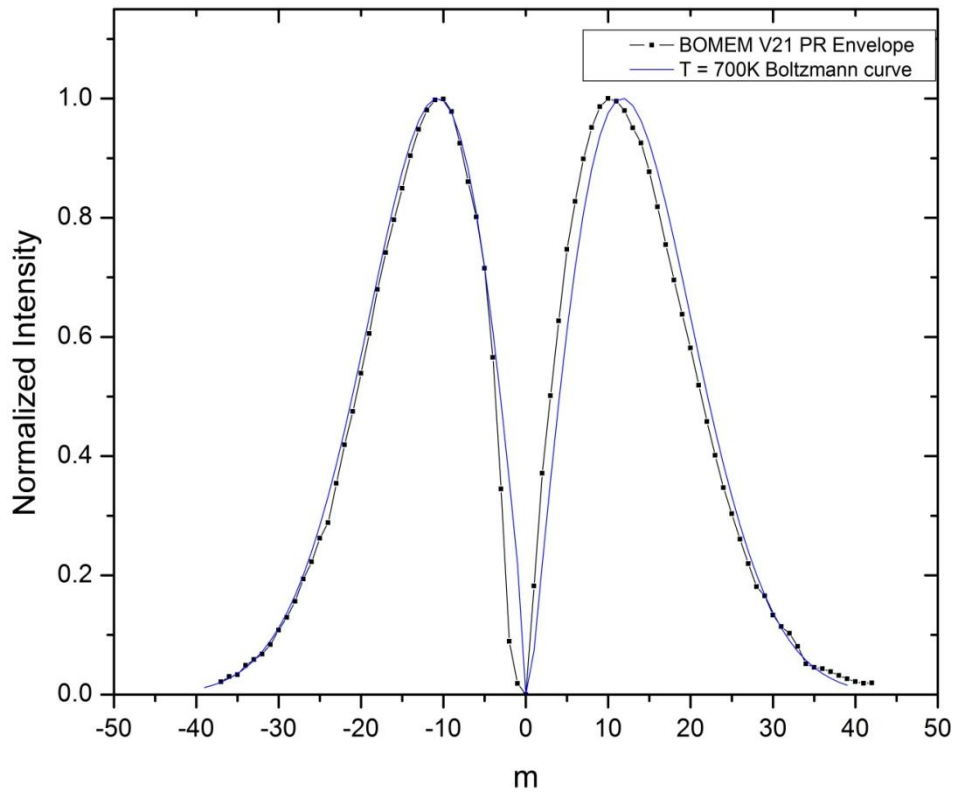

Figure 19. Theoretical and experimental envelop function for the P and R branches of V(21).

3.7 The synthetic spectrum of V(21) transition

Our goal is to simplify the spectrum as much as possible by subtracting synthetic spectra for transitions that we have succeeded in identifying. It seems knowing the parameters such as rotational temperature and linewidth, enables us to generate the synthetic spectrum for these known transitions. The result would be a simpler spectrum which could be beneficial for finding new transitions in the empirical spectrum. To achieve this goal, the synthetic spectrum of V(21) transition has been generated, using a short program in FORTRAN90 and assumption of T_{tran} = 290 K. A Gaussian profile for each rotational peak has been used. Fig. 20 shows the final synthetic spectrum plotted together with the original empirical data:

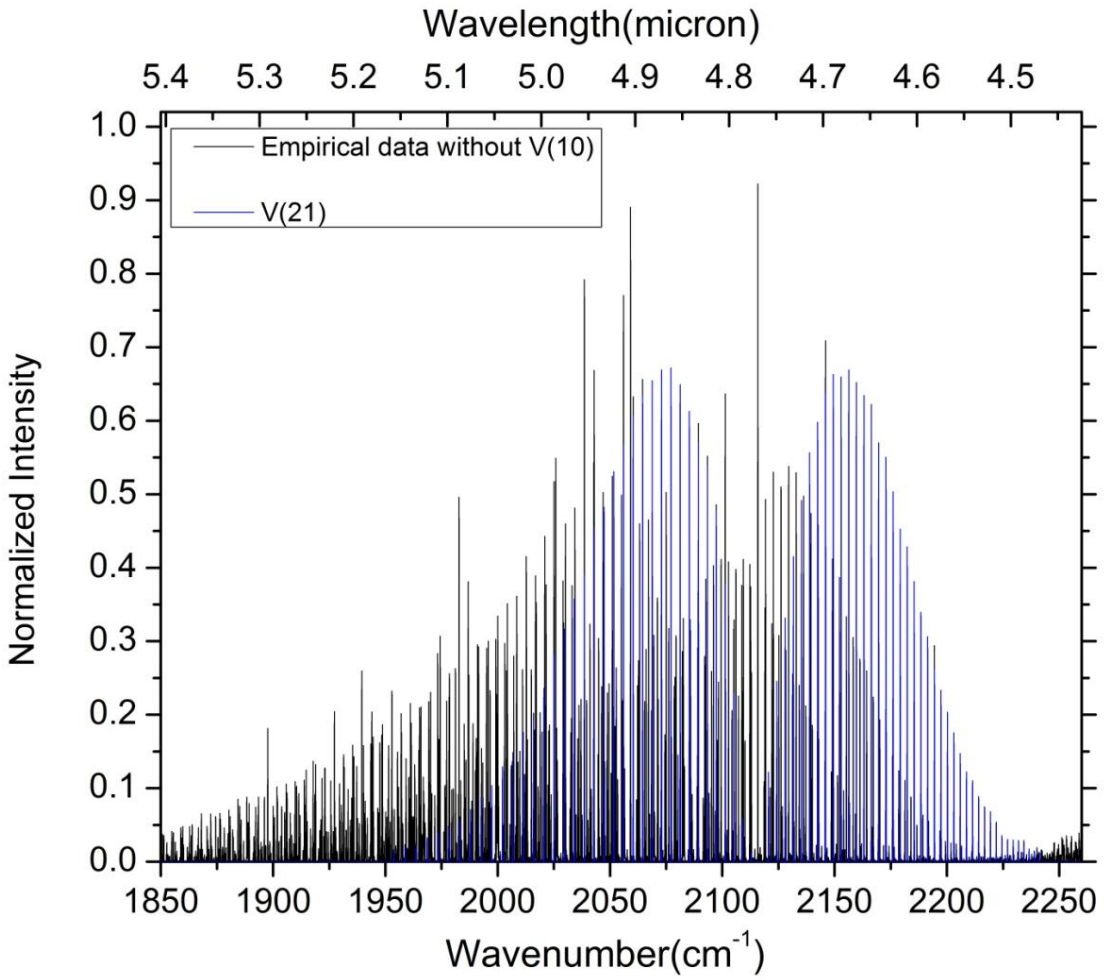

Figure 20. V(21) synthetic spectrum plotted together with empirical data.

Generating the synthetic spectrum and subtracting it from the empirical data, gives us the subtracted spectrum with less lines than the original spectrum. The same method could be applied for identifying other unknown transitions in the spectrum.

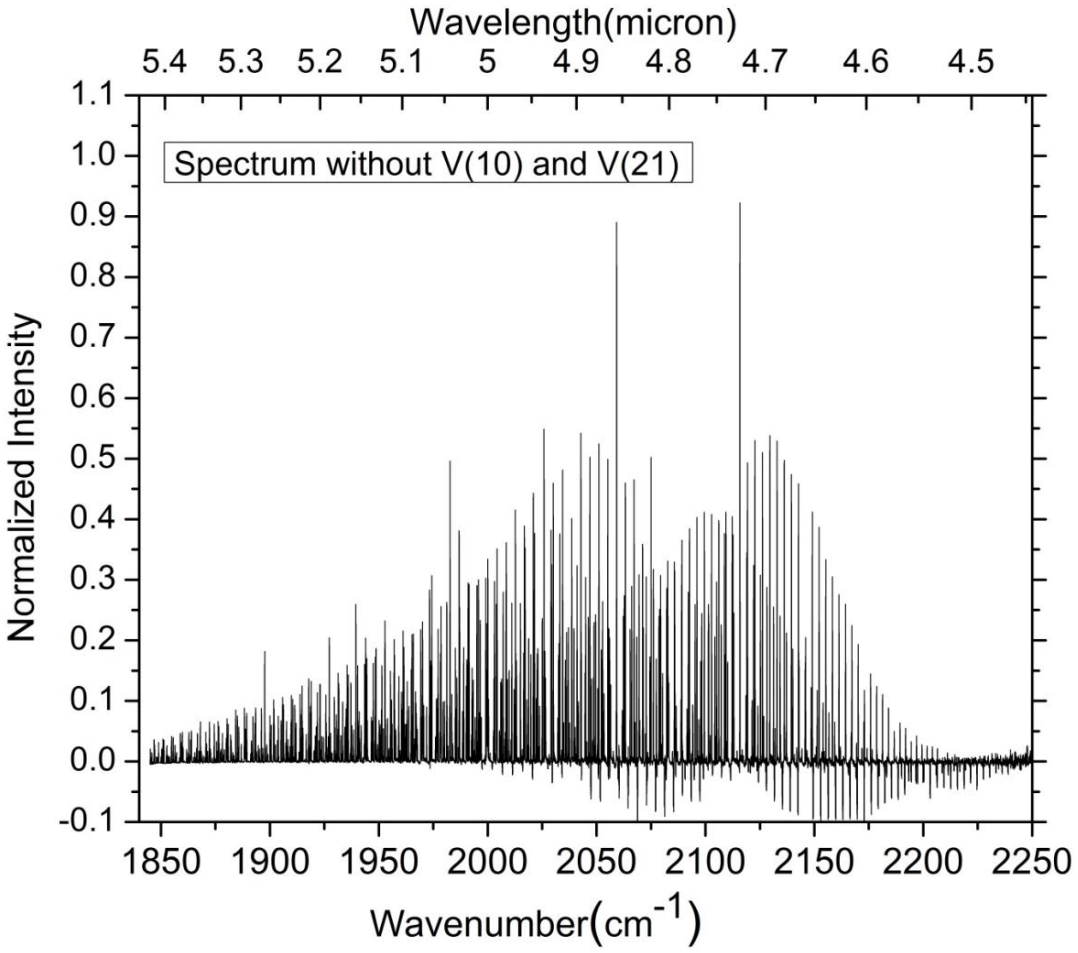

Figure 21. Final spectrum after subtraction of V(10) and V(21).

As it is shown in Fig 21, the subtracted spectrum has a simpler shape than the original spectrum. As a consequence of the subtraction, the bands (other than V(10) and V(21)) that were hard to see in the original spectrum are more recognizable.

CHATER FOUR: SUMMARY

High temperature emission spectrum of Carbon Monoxide, which is an important molecule in different astronomical objects and has recently got a lot of attention in the scientific community, has been presented. The data was obtained using a BOMEM DA8 spectrometer in a microwave discharged apparatus with a source of CO_2, which was being dissociated to CO.

To investigate the effects of disequilibrium on the emission spectra, the spectrum of hot CO was obtained in experiments with a high level of ionization and reactive fragments in a microwave discharge apparatus. Vibrational transitions originating in up to the 13^{th} vibrational level of the $X\ ^1\Sigma^+$ ground electronic term were observed. From the J values for maximum intensity lines within the rotational fine structure, we obtain a temperature estimate of ~700 K.

The results clearly show emission lines the fundamental vibration of CO molecule V(10) in both P and R bands up to J = 38. The rotational temperature of CO molecules in V(10) emission was estimated in the order of 700 K while from the width of rotational states, the translational temperature of CO molecules were estimated to be around 290 K. In addition, the V(21) emission lines of CO molecule centering around 2120 cm^{-1} were observed in the spectrum up to J = 36. Other transition with $\Delta V = -1$ where observed and matched with current lines list of CO in ground electronic state up to V = 13.

For identifying the other possible transitions in the spectrum, the synthetic spectra of V(10) and V(21) were generated. For each of these transitions, relative intensities of corresponding rotational states were obtained and matched with the empirical data. For the peaks with overlapped transitions, relative intensity was adjusted by interpolation method. The lineshape of each rotational state was generated by adjusting the width of the peaks to the empirical width assuming the dominating effect of Doppler broadening in the discharge tube. The subtraction of transitions V(10) and V(21) from the empirical data have been performed. The subtracted spectrum shows much cleaner lines comparing to original one. This spectrum may be helpful in identifying other unknown transitions in the spectrum. Further work must be done to identify the origin of the observed transitions in the spectrum.

APPENDIX A:
INTENSITIES OF V(10) AND V(21) TRANSITIONS

Table 1 - Corresponding R-branch of V(10) transition and its relative intensities

PEAK center (cm^{-1})	INTESNSITY	R-BRANCH
2147.047	0.174	R0
2150.817	0.195	R1
2154.582	0.195	R2
2158.288	0.496	R3
2161.934	0.215	R4
2165.581	0.209	R5
2169.166	0.207	R6
2172.782	0.232	R7
2176.247	0.223	R8
2179.743	0.236	R9
2183.208	0.234	R10
2186.613	0.285	R11
2189.988	0.258	R12
2193.332	0.272	R13
2196.64	0.281	R14
2203.126	0.472	R16
2206.319	0.321	R17
2209.483	0.330	R18
2212.588	0.318	R19
2215.690	0.316	R20

PEAK center (cm^{-1})	INTESNSITY	R-BRANCH
2218.731	0.298	R21
2221.718	0.300	R22
2224.699	0.271	R23
2227.624	0.256	R24
2230.515	0.219	R25
2233.348	0.221	R26
2236.150	0.185	R27
2238.922	0.182	R28
2241.664	0.164	R29
2244.346	0.150	R30
2246.997	0.131	R31
2249.620	0.133	R32
2252.210	0.128	R33
2254.742	0.101	R34
2257.213	0.123	R35
2259.654	0.139	R36
2262.124	0.099	R37
2264.414	0.11	R38

Table 2 Corresponding P-branch of V(10) transition and its relative intensities

PEAK center (cm^{-1})	INTESNSITY	P-BRANCH
2139.456	0.656	P1
2135.508	0.196	P2
2131.651	0.569	P3
2127.643	0.219	P4
2123.666	0.224	P5
2119.658	0.223	P6
2115.590	0.229	P7
2111.523	0.234	P8
2107.395	0.247	P9
2103.236	0.264	P10
2099.049	0.269	P11
2094.831	0.285	P12
2090.581	0.303	P13
2086.302	0.322	P14
2081.964	0.329	P15
2077.624	0.357	P16
2073.225	0.357	P17
2068.795	0.915	P18
2064.366	0.373	P19
2059.876	0.357	P20

PEAK center (cm^{-1})	INTESNSITY	P-BRANCH
2055.386	0.343	P21
2050.836	0.329	P22
2046.256	0.533	P23
2041.677	0.351	P24
2037.094	0.437	P25
2032.335	0.222	P26
2027.635	0.204	P27
2022.902	0.186	P28
2018.112	0.168	P29
2013.321	0.191	P30
2008.531	0.499	P31
2003.650	0.130	P32
1998.768	0.129	P33
1993.857	0.114	P34
1988.915	0.165	P35
1983.943	0.134	P36
1978.910	0.106	P37
1973.8	0.08	P38
1968.815	0.094	P39

Table 3 Corresponding R branch of V(21) and its relative intensities

PEAK center (cm^{-1})	INTESNSITY	R-BRANCH
2120.5329	0.198	R0
2124.269	0.317	R1
2127.976	0.398	R2
2131.651	0.569	R3
2135.2979	0.552	R4
2138.883	0.618	R5
2142.439	0.659	R6
2145.964	0.784	R7
2149.459	0.722	R8
2152.925	0.719	R9
2156.330	0.732	R10
2159.705	0.714	R11
2163.049	0.696	R12
2166.364	0.680	R13
2169.619	0.624	R14
2172.872	0.622	R15
2176.067	0.572	R16
2179.230	0.515	R17
2182.334	0.490	R18
2185.407	0.442	R19

PEAK center (cm^{-1})	INTESNSITY	R-BRANCH
2188.451	0.399	R20
2191.464	0.370	R21
2194.447	0.368	R22
2197.370	0.304	R23
2200.262	0.274	R24
2203.125	0.472	R25
2205.927	0.219	R26
2208.700	0.197	R27
2211.442	0.179	R28
2214.123	0.160	R29
2216.775	0.145	R30
2219.397	0.139	R31
2219.397	0.139	R32
2221.988	0.128	R33
2224.519	0.115	R34
2227.020	0.105	R35
2229.491	0.108	R36
2231.902	0.106	R37
2234.282	0.106	R38
2236.603	0.092	R39
2238.922	0.182	R40

Table 4 Corresponding P branch of V(21) transition and its relative intensities

PEAK center (cm^{-1})	INTESNSITY	P-BRANCH
2112.969	0.336	P1
2109.112	0.309	P2
2105.225	0.409	P3
2101.307	0.716	P4
2097.361	0.566	P5
2093.384	0.631	P6
2089.375	0.676	P7
2085.308	0.691	P8
2081.240	0.718	P9
2077.112	0.740	P10
2072.953	0.727	P11
2068.795	0.916	P12
2064.547	0.739	P13
2060.298	0.716	P14
2056.019	0.853	P15
2051.710	0.602	P16
2047.341	0.552	P17
2042.972	0.753	P18
2038.572	0.877	P19
2034.112	0.441	P20

PEAK center (cm^{-1})	INTESNSITY	P BRANCH
2029.623	0.397	P21
2025.073	0.603	P22
2020.584	0.317	P23
2016.003	0.288	P24
2011.393	0.258	P25
2006.752	0.230	P26
2002.082	0.213	P27
1997.382	0.187	P28
1992.651	0.173	P29
1987.890	0.158	P30
1983.099	0.148	P31
1978.338	0.312	P32
1973.4	0.09	P33
1968.544	0.120	P34
1963.634	0.114	P35
1958.7	0.11	P36

APPENDIX B:
OBSERVED VIBRATIONAL-ROTATIONAL TRANSITIONS IN THE SPECTRUM

In this appendix, the entire empirical emission spectrum is presented in 20 cm^{-1} blocks. Vibrational transitions of CO molecule with $\Delta V = -1$ and up to $V = 13$ have been marked on the empirical spectrum using the Goorvitch linelist [17] and CO laser lines [20].

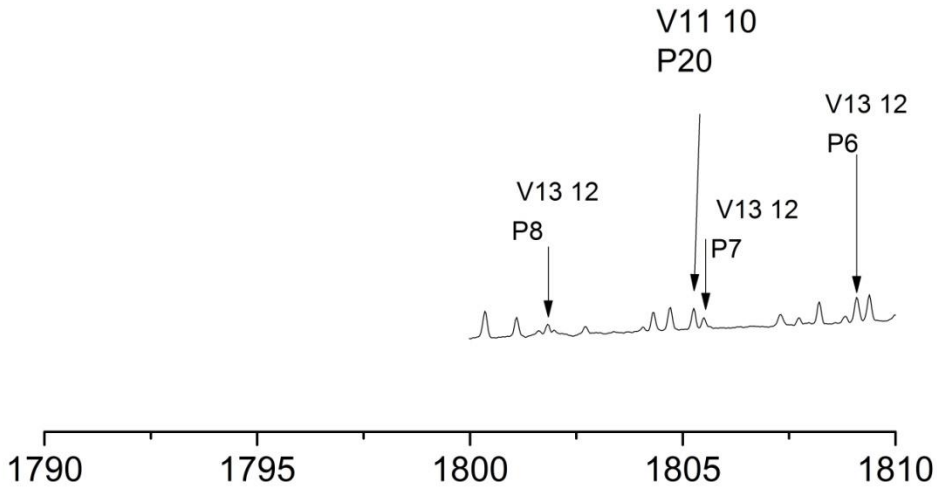

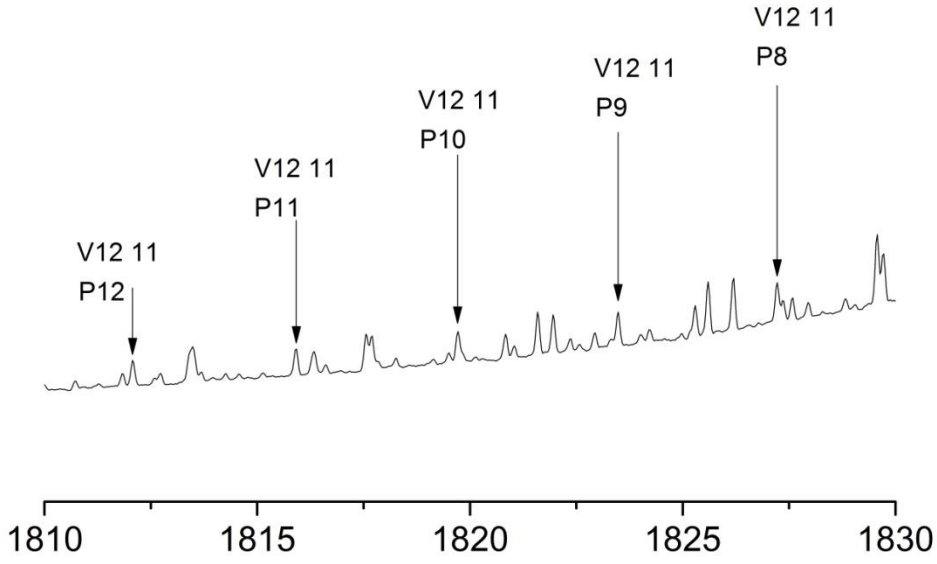
V12 11
P12
V12 11
P11
V12 11
P10
V12 11
P9
V12 11
P8
1810
1815
1820
1825
1830

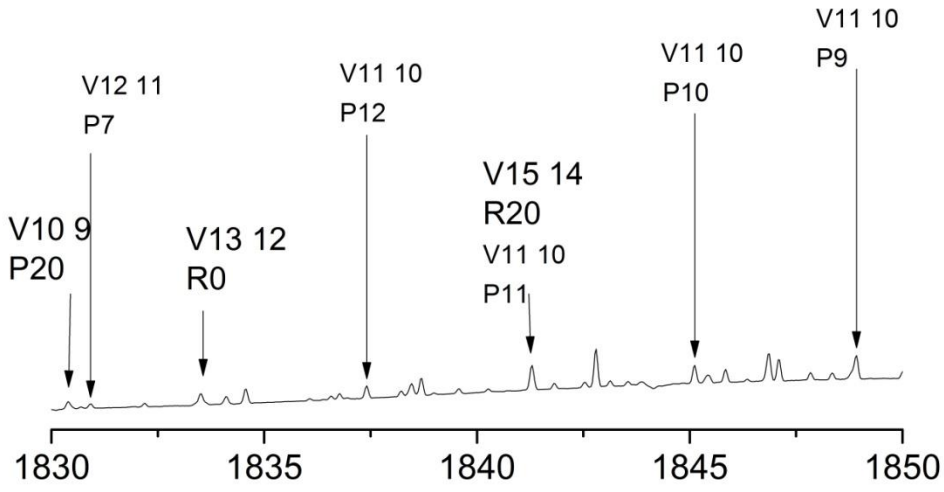
V10 9
P20
V12 11
P7
V13 12
R0
V11 10
P12
V15 14
R20
V11 10
P11
V11 10
P10
V11 10
P9
1830
1835
1840
1845
1850

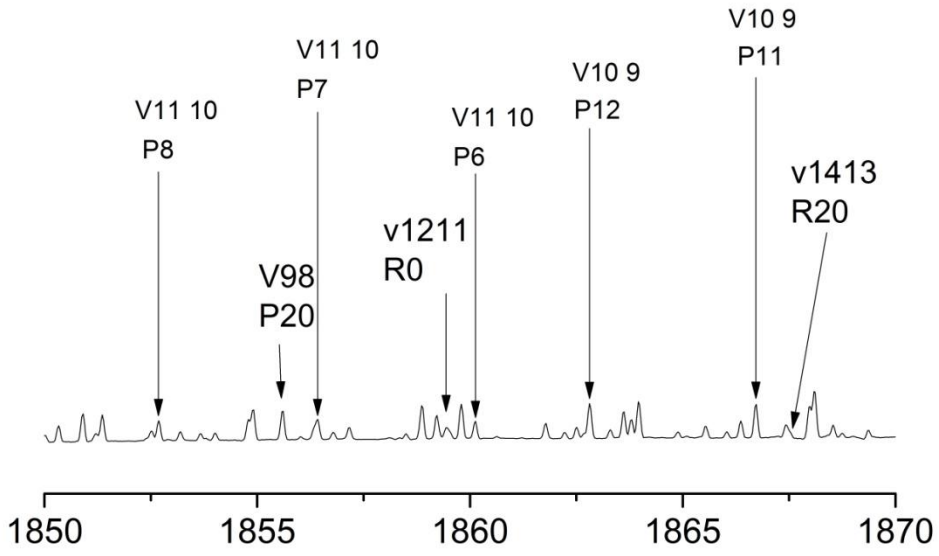
V11 10
P8
V11 10
P7
V98
P20
v1211
R0
V11 10
P6
V10 9
P12
V10 9
P11
v1413
R20
1850
1855
1860
1865
1870

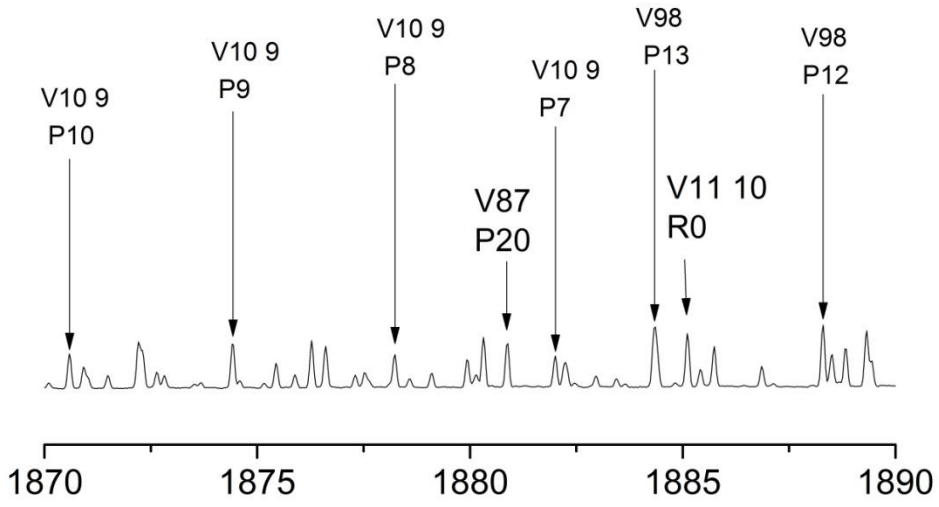
V10 9
P10
V10 9
P9
V10 9
P8
V87
P20
V10 9
P7
V98
P13
V11 10
R0
V98
P12
1870
1875
1880
1885
1890

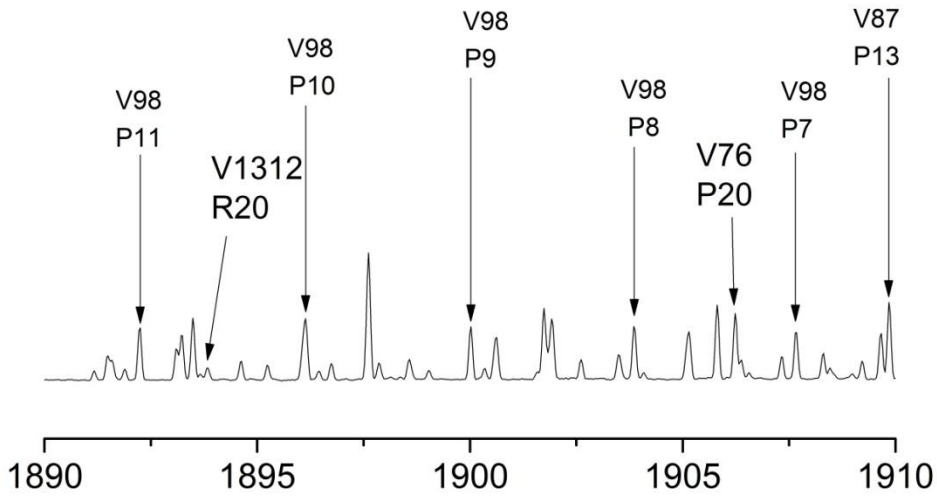
V98
P11
V98
P10
V1312
R20
V98
P9
V98
P8
V76
P20
V98
P7
V87
P13
1890
1895
1900
1905
1910

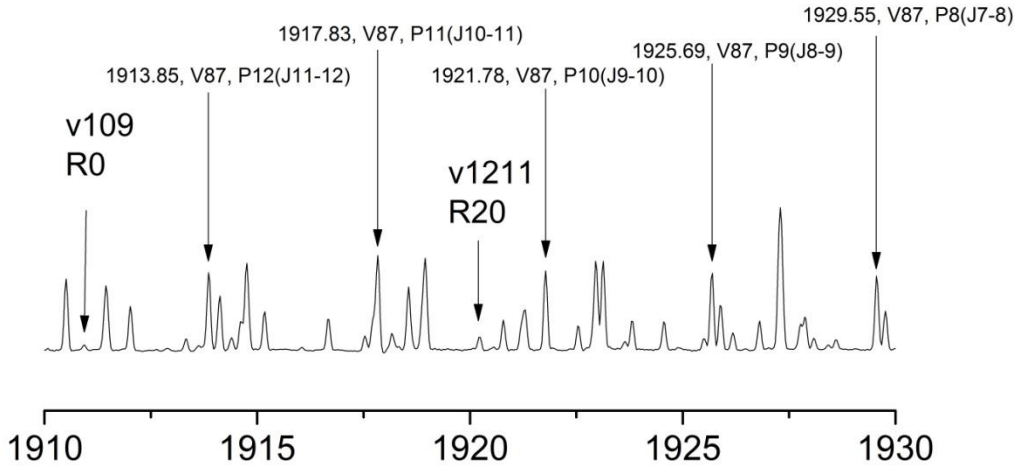
1929.55, V87, P8(J7-8)
1917.83, V87, P11(J10-11)
1925.69, V87, P9(J8-9)
1913.85, V87, P12(J11-12)
1921.78, V87, P10(J9-10)
v109
R0
v1211
R20
1910
1915
1920
1925
1930

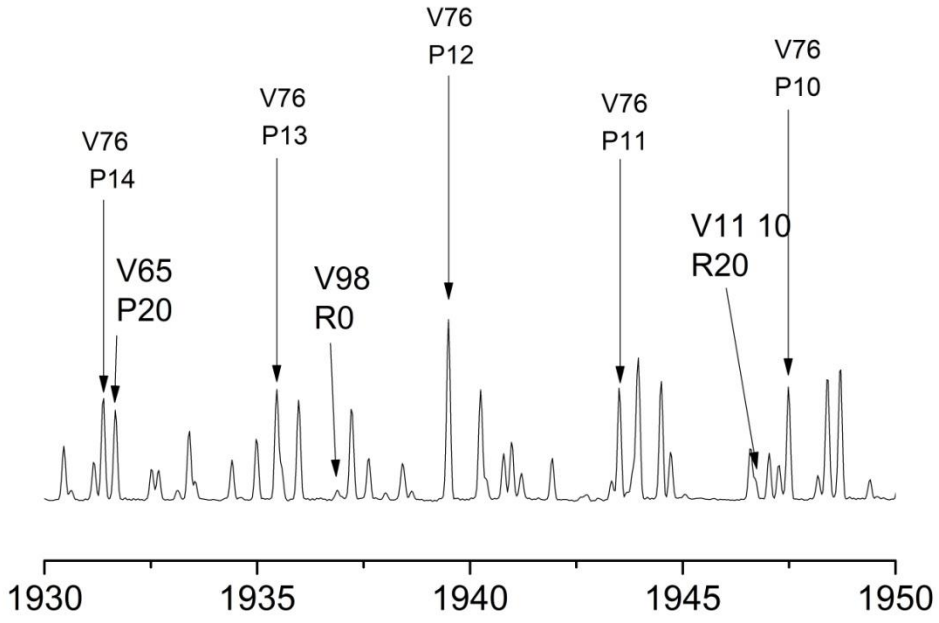
V76
P14
V65
P20
V76
P13
V98
R0
V76
P12
V76
P11
V11 10
R20
V76
P10
1930
1935
1940
1945
1950

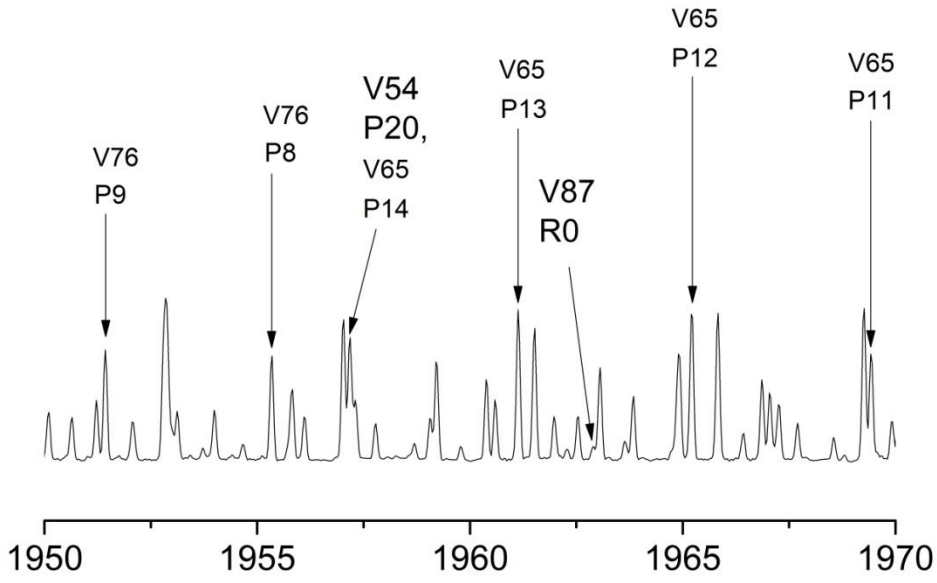
V76
P9
V76
P8
V54
P20,
V65
P14
V65
P13
V87
R0
V65
P12
V65
P11
1950
1955
1960
1965
1970

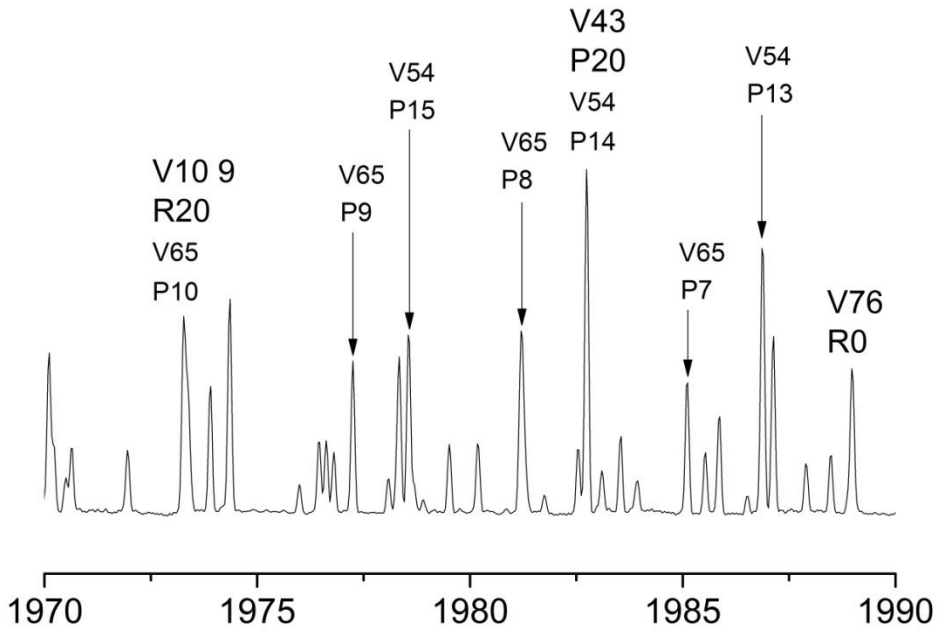
V10 9
R20
V65
P10
V65
P9
V54
P15
V65
P8
V43
P20
V54
P14
V65
P7
V54
P13
V76
R0
1970
1975
1980
1985
1990

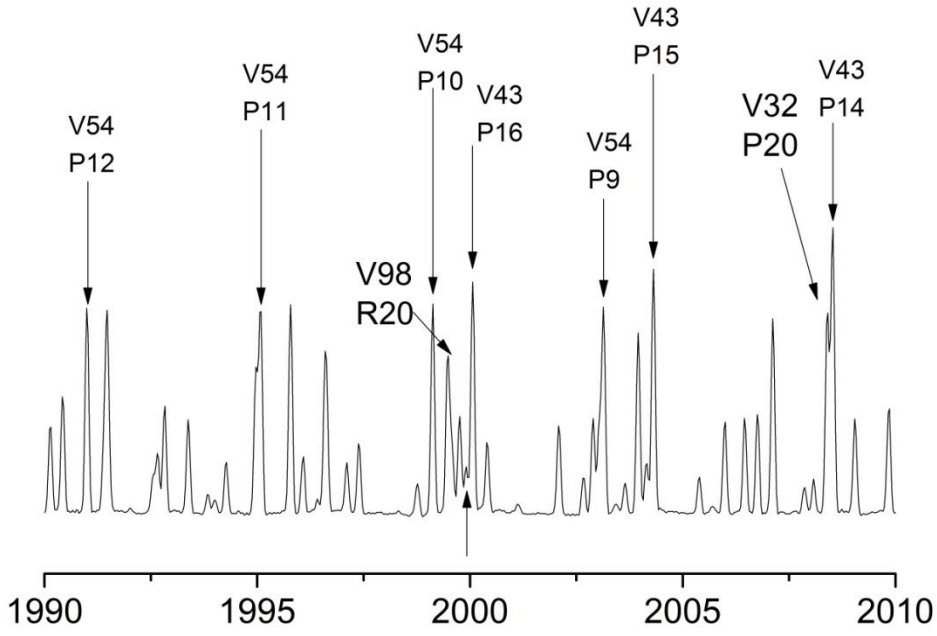
V54
P12
V54
P11
V54
P10
V43
P16
V98
R20
V54
P9
V43
P15
V32
P20
V43
P14
1990
1995
2000
2005
2010

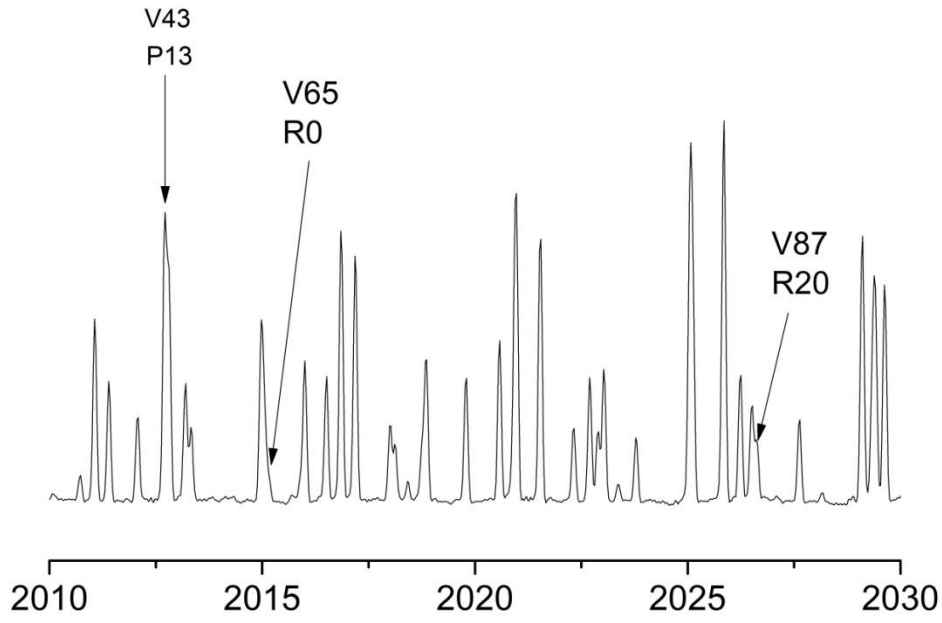
V43
P13
V65
R0
V87
R20
2010
2015
2020
2025
2030

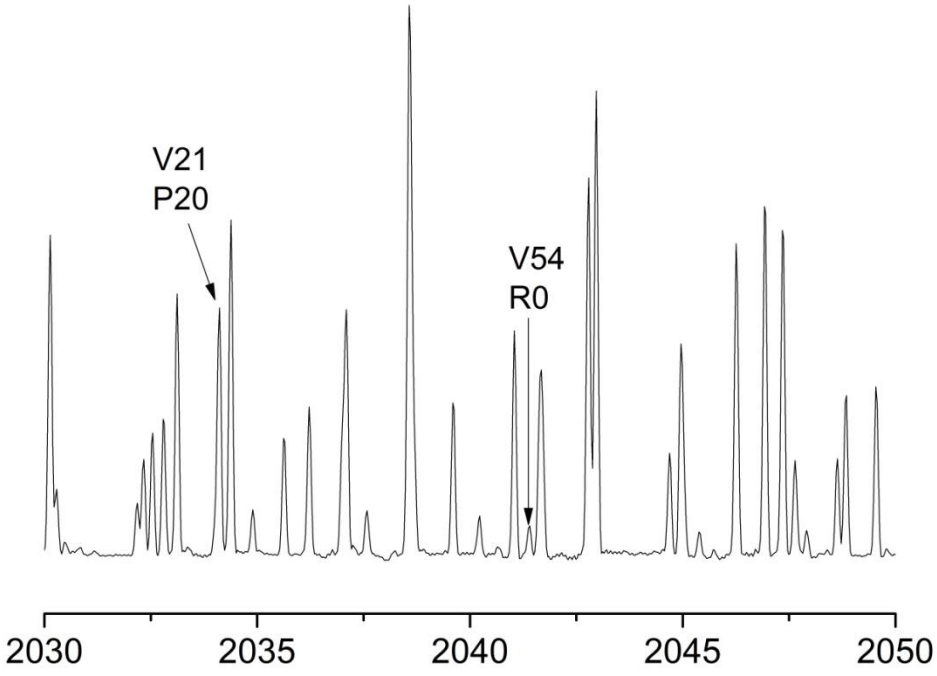
V21
P20
V54
R0
2030
2035
2040
2045
2050

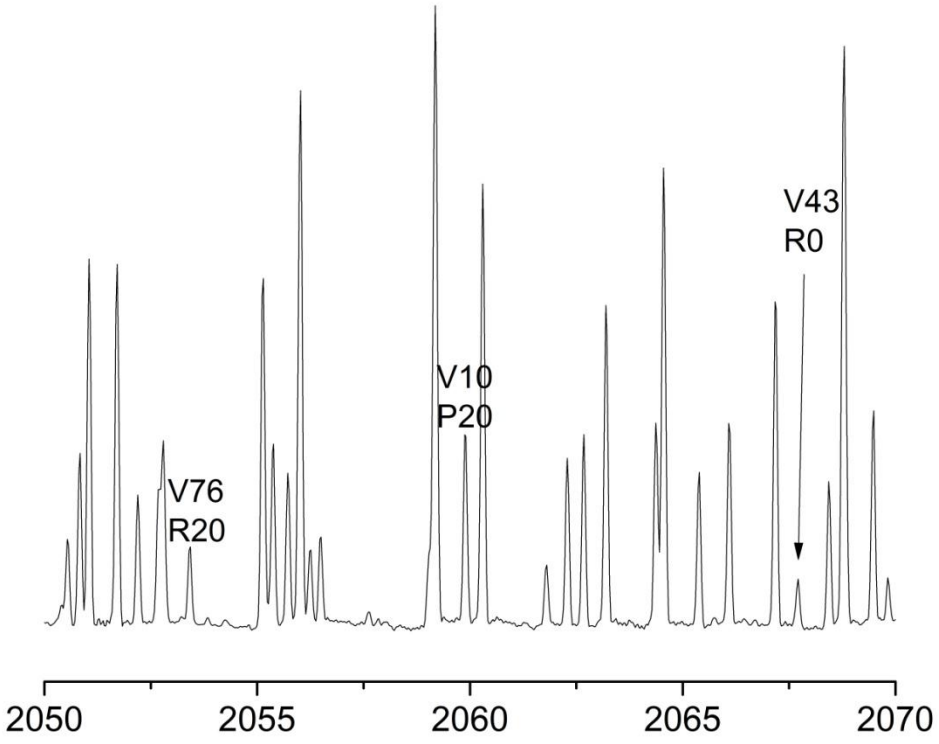
V43
R0
V10
P20
V76
R20
2050
2055
2060
2065
2070

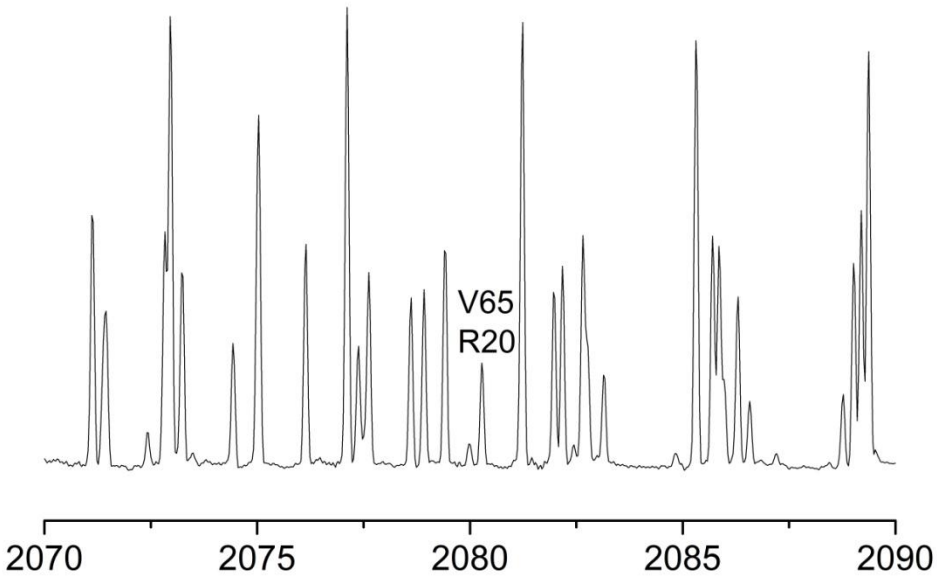
V65
R20
2070
2075
2080
2085
2090

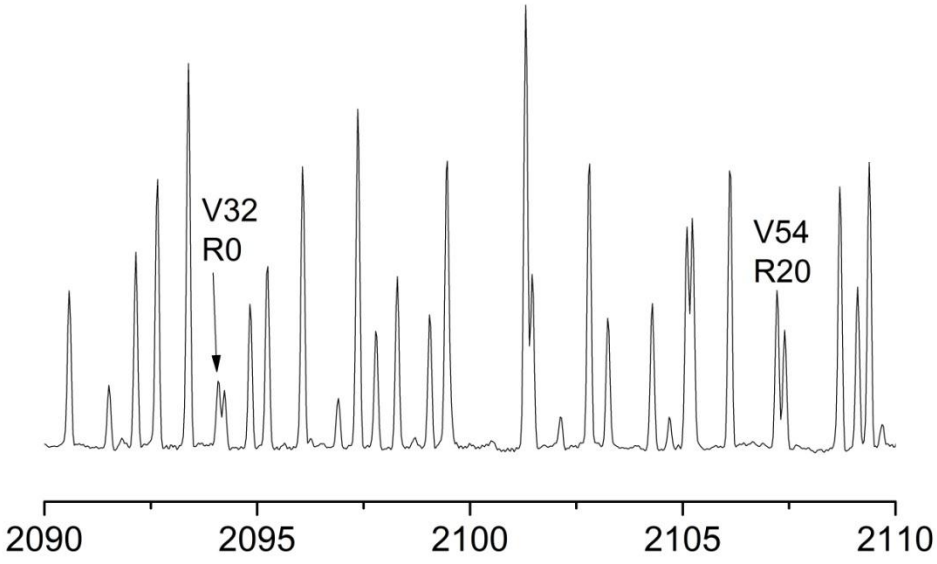
V32
R0
V54
R20
2090
2095
2100
2105
2110

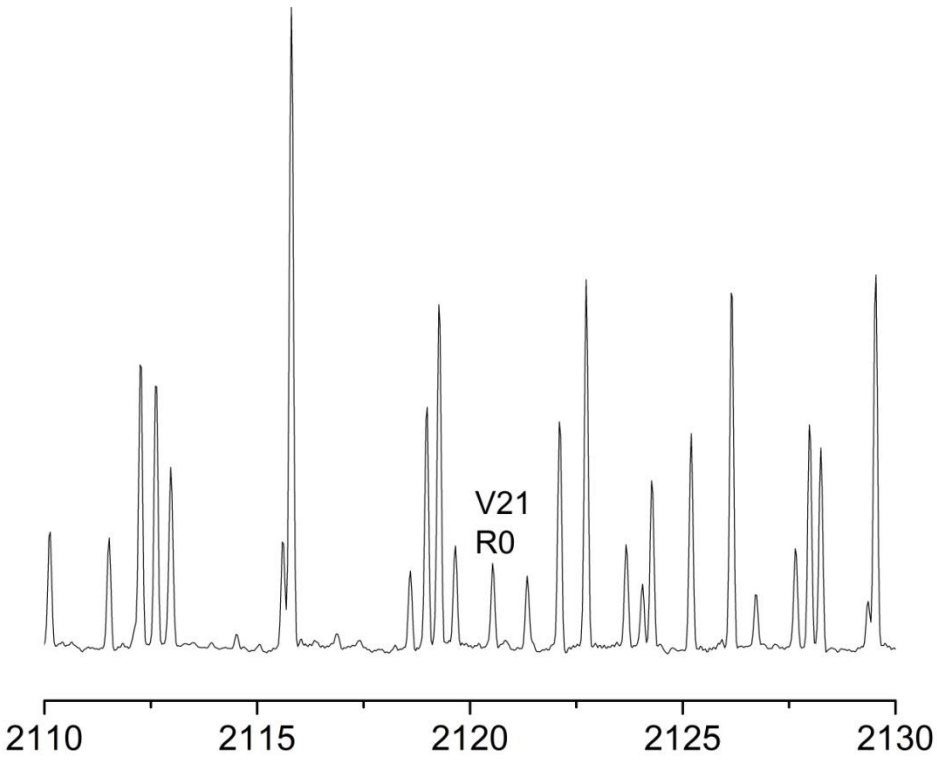
V21
R0
2110
2115
2120
2125
2130

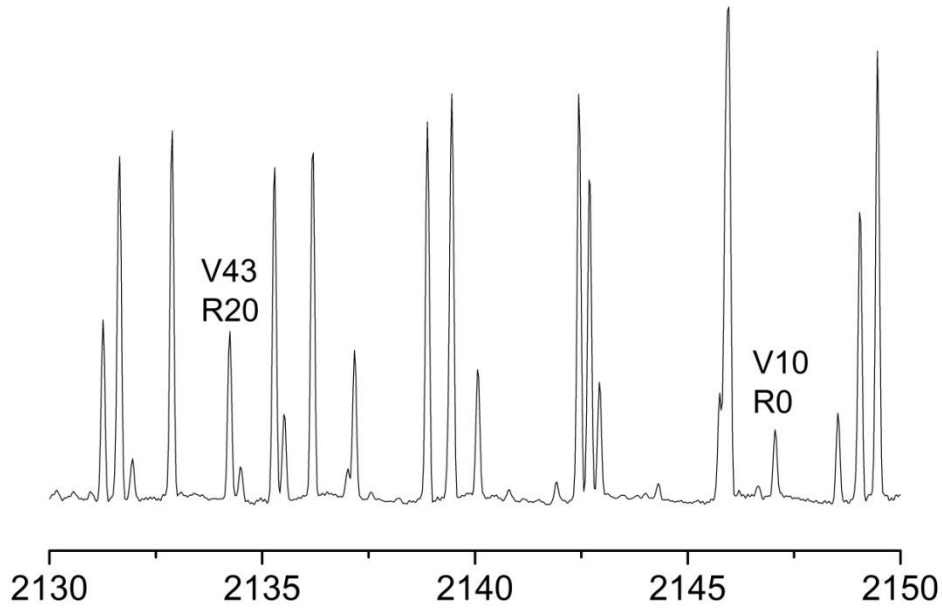
V43
R20
V10
R0
2130
2135
2140
2145
2150

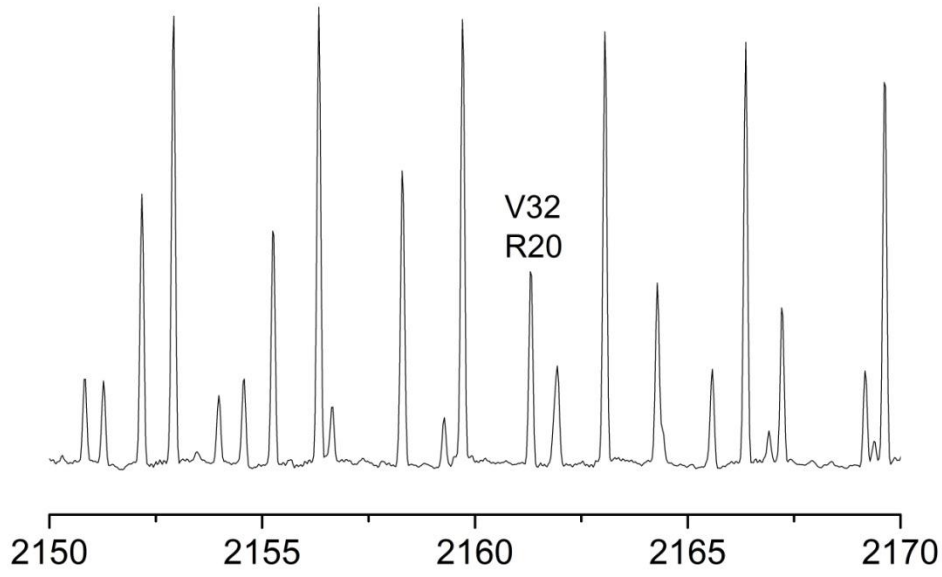
V32
R20
2150
2155
2160
2165
2170

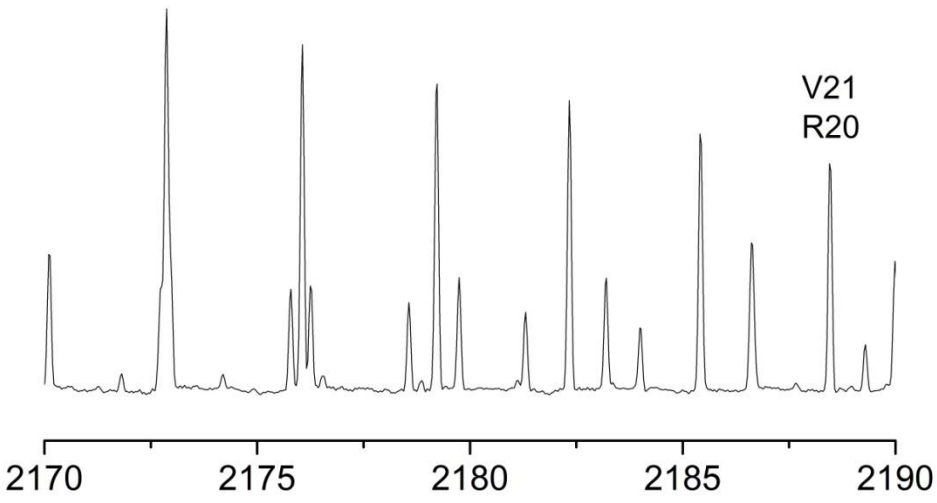
V21
R20
2170
2175
2180
2185
2190

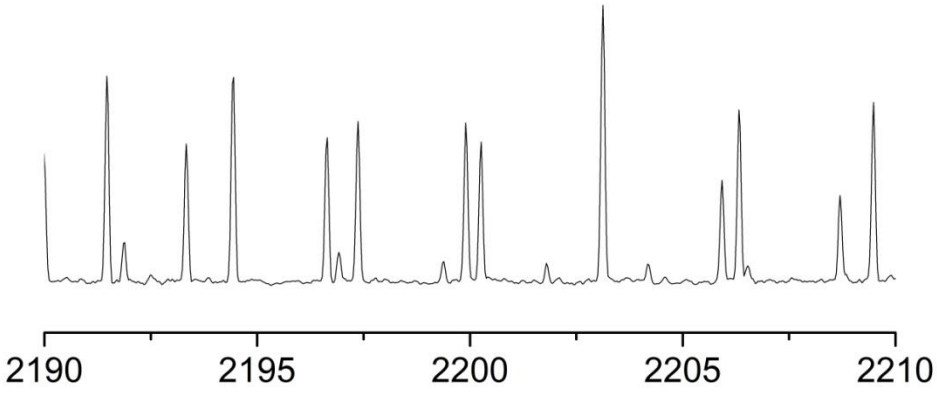
2190
2195
2200
2205
2210

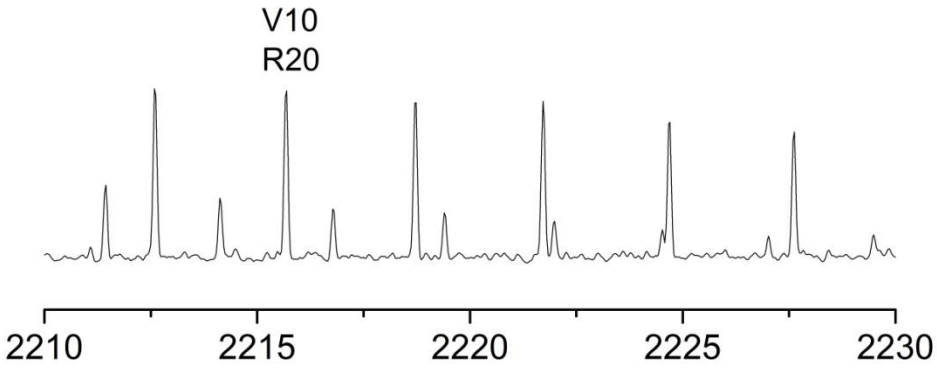
V10
R20
2210
2215
2220
2225
2230

LIST OF REFRENCES

[1] Cameron A.C., March 2007, Monthly Notices of the Royal Astronomical Society, Volume 375, Issue 3, pages 951–957

[2] The HITRAN 2004 molecular spectroscopic database, Journal of Quantitative Spectroscopy & Radiative Transfer 96 ,139–204

[3]http://www.Spectra factory.net

[4] Najita, J. R., Carr, J. S., Glassgold, A. E., & Valenti, J. A. 2007, Protostars and Planets V, ed. B. Reipurth

[5] Thompson, R. I. 1985, ApJ, 299, L41

[6] Carr, J. S. 1989, ApJ, 345, 522

[7] Najita, J., Carr, J. S., & Mathieu, R. D. 2003, ApJ, 589, 931

[8] Salyk, C., Blake, G. A., Boogert, A. C. A., & Brown, J.M. 2007, ApJ, 655, L105

[9] Brittain, S. D., Rettig, T. W., Simon, T., Kulesa, C., DiSanti, M. A., & Dello Russo, N. 2003, ApJ, 588, 535

[10] Blake, G. A., & Boogert, A. C. A. 2004, ApJ, 606, L73

[11] Bast J.E.,Brown M.J.,Herczeg G.J.,Van Dishoeck E.F.,Pontoppidan K.M., 2011, Single peaked CO emission line profiles from the inner regions of protoplanetary disks, AA manuscript, 15225

[12] Tappe A.; Forbrich, J.; Martin; Lada, C. J., The Anatomy of the Young Protostellar Outflow HH 211: Strong Evidence for CO v = 1-0 Fundamental Band Emission from Dense Gas in the Terminal Shock, American Astronomical Society, AAS Meeting #218, #226.07

[13] Landau L.D., Lifshitz L.M., Quantum Mechanics: Course of theoretical physics, vol.3, Butterworth Heinmann, Burlingthon, MA,1977

[14] Kneba, M. and Wolfrum, J., 1980, “Bimolecular Reactions of Vibrationally Excited Molecules”, Ann. Rev. Phys. Chem., Vol. 31, pp. 47-79.

[15] Huber K.P. and Herzberg G., Molecular spectra and molecular structure(constants of diatomic molecule),Van Norstand, Princeton, New Jersey,1979

[16] Demtroder W., Laser spectroscopy, Springer-Verlag, Berlin, 1988

[17] Goorvitch D., 1994, APJ supplement series,95:535-552

[18] Herzberg G., Molecular spectra and molecular structure, Van Norstand, Princeton, New Jersey,1950

[19] Handbook of Military infrared technology, Wolfe W.E., Office of Naval research, department of the Navy, Washington, D.C., 1965

[20] Yardley T.J., 1970, Laser action in highly excited vibrational levels of CO, Journal of molecular spectroscopy, 35: 314-324